HIGH ENERGY PHOTO-EJECTION OF NEUTRON-PROTON PAIRS FROM VARIOUS NUCLEI

Henry Hamilton Wilson

HIGH ENERGY PHOTO-EJECTION OF NEUTRON-PROTON PAIRS FROM VARIOUS NUCLEI

by

HENRY HAMILTON WILSON

B.S., United States Naval Academy

(1947)

SUBMITTED IN PARTIAL FULFILLMENT OF THE

REQUIREMENTS FOR THE DEGREE OF

MASTER OF SCIENCE

at the

MASSACHUSETTS INSTITUTE OF TECHNOLOGY

June, 1955

Signature of Author...
Department of Physics, May 23, 1955

Certified by...
Thesis Supervisor

Accepted by...
Chairman, Departmental Committee on Graduate Students

W636

HIGH ENERGY PHOTO-PRODUCTION OF NEUTRON-PROTON PAIRS FROM VARIOUS NUCLEI

by

SIDNEY HAMILTON WILSON

B.S., United States Naval Academy

(1947)

SUBMITTED IN PARTIAL FULFILLMENT OF THE

REQUIREMENTS FOR THE DEGREE OF

MASTER OF SCIENCE

at the

MASSACHUSETTS INSTITUTE OF TECHNOLOGY

June, 1955

Signature of Author...
Department of Physics, May 23, 1955

Certified by...
Thesis Supervisor

Accepted by...
Chairman, Departmental Committee on Graduate Students

ABSTRACT

HIGH ENERGY PHOTO-EJECTION OF NEUTRON-PROTON
PAIRS FROM VARIOUS NUCLEI
by
HENRY HAMILTON WILSON

Submitted to the Department of Physics on May 23, 1955 in partial fulfillment of the requirements for the degree of Master of Science

Neutrons have been observed in coincidence with high energy photoprotons in this and other laboratories. For a fixed proton energy and angle the neutrons detected in coincidence with these protons possess an angular distribution about the angle predicted for the ejection of the neutron by the kinematics of a gamma ray interaction with a deuteron at rest. The neutrons in coincidence with photoprotons at angles beyond those expected from the resolution of the detectors can arise from initial nucleon momenta. This suggested that the shape of these neutron angular distributions could be employed as a mode of studying the average momenta and perhaps the momentum distributions of nucleons in different nuclei.

Curves were taken for deuterium, lithium, carbon, oxygen, aluminum and copper. The deuterium curve was taken as an experimental check on the resolution of the equipment. A finite angular spread was noted in lithium beyond that due to the resolution of the detectors. A marked increase in the angular spread occurred between lithium and carbon with a slight further increase for aluminum and copper.

A crude theory has been developed for the shape of these curves. A three-dimensional gaussian distribution is assumed. It was fitted to the lithium data with a 1/e value of approximately 9 Mev and to carbon and oxygen with a 1/e value of approximately 19 Mev. The aluminum and copper do not fit the theoretical shape. The possibility exists that neutrons scattered within the nucleus broaden such curves in these nuclei.

Thesis Supervisor: Bernard T. Feld
Title: Associate Professor of Physics

ABSTRACT

HIGH ENERGY PHOTO-EJECTION OF NEUTRON-PROTON PAIRS FROM VARIOUS NUCLEI

by

ROBERT [illegible] WILSON

Submitted to the Department of Physics on May 23, 1955 in partial fulfillment of the requirements for the degree of Master of Science

Neutrons have been observed in coincidence with high energy photoprotons in this and other laboratories. For a fixed proton energy and angle the neutrons detected in coincidence with these protons possess an angular distribution about the angle predicted for the ejection of the neutron by the kinematics of a gamma ray interaction with a deuteron at rest. The neutrons in coincidence with photoprotons at angles beyond those expected from the resolution of the detectors can arise from initial nucleon momenta. This suggested that the shape of these neutron angular distributions could be employed as a mode of studying the average momenta and perhaps the momentum distributions of nucleons in different nuclei.

Curves were taken for deuterium, lithium, carbon, oxygen, aluminum and copper. The deuterium curve was taken as an experimental check on the resolution of the equipment. Finite angular spread was noted in lithium beyond that due to the resolution of the detectors. A marked increase in the angular spread occurred between lithium and carbon with a slight further increase for aluminum and copper.

A crude theory has been developed for the shape of these curves. A three-dimensional gaussian distribution is assumed. It was fitted to the lithium data with a 1/e value of approximately 9 Mev and to carbon and oxygen with a 1/e value of approximately 19 Mev. The aluminum and copper do not fit this theoretical shape. The possibility exists that neutrons scattered within the nucleus broaden such curves in these nuclei.

Thesis Supervisor: Bernard T. Feld
Title: Associate Professor of Physics

ACKNOWLEDGEMENTS

I am deeply indebted to Dr. Albert Wattenberg and Professor Bernard T. Feld for constant guidance and valuable support in the theoretical aspects of this work. Allen Odian, Peter Stein and Dr. Roy Weinstein ably assisted in the preparation of the equipment and during the measurements. Thanks are also due to William Rankin and Eugene Christie for assistance during the measurements.

This work was in part supported jointly by the Atomic Energy Commission and the Office of Naval Research.

ACKNOWLEDGMENT

I am deeply indebted to Dr. Albert [illegible] and
[illegible]rofessor Bernard T. Feld for constant guidance and valuable
[illegible]upport in the theoretical aspects of this work. [illegible]
[illegible]eter Stein and Dr. Roy Weinstein ably assisted in the prepa-
[illegible]ration of the equipment and during the measurements. Thanks
[illegible]re also due to William [illegible] and Eugene [illegible] for
[illegible]ssistance during the measurements.

This work was in part supported jointly by the Atomic
[illegible]nergy Commission and the Office of Naval Research.

TABLE OF CONTENTS

TABLE OF CONTENTS

INDEX TO DRAWINGS

INDEX TO DRAWINGS

INDEX TO TABLES

INDEX OF TABLES

I. Introduction

A. Photo-Nuclear Processes

The production of photoprotons as a result of the reaction of gamma rays with different nuclei has been studied by many investigators[1]. The types of interactions of gamma rays with nuclei by which the photoprotons are produced vary with the energy of the gamma ray[2]. In the region of higher photon energies above approximately 100 Mev the predominant reaction results in an ejected proton which frequently possesses an energy comparable to that of the incident gamma ray. The common method of observing these higher energy reactions has been to bombard the target nuclei with high energy x-rays from bremsstrahlung sources. Because the bremsstrahlung spectrum falls off rapidly with increasing energy the strong weighting of lower energy protons makes interpretation of the observations difficult.

However, numerous observations have resulted in a large amount of information on high energy protons from x-rays on various targets. Protons of energies between 10 and 70 Mev were studied by Levinthal and Silverman[3] using the 322 Mev Berkeley synchrotron yielding a proton energy spectrum which fell off roughly as E^{-2}. While the 10 Mev protons were ejected isotropically (probably the tail of the evaporation spectra) the 40 Mev protons showed a distinct forward peaking in angular distribution. Walker[4] employed a 195 Mev x-ray beam from the Cornell synchrotron to observe protons of energies greater than about 70 Mev. He observed a forward peaking in the angular distribution and a more rapid decrease with energy of about

I. Introduction

A. Photo-Nuclear Processes

The production of photoprotons as a result of the reaction of gamma rays with different nuclei has been studied by many investigators[1]. The types of interactions of gamma rays with nuclei by which the photoprotons are produced vary with the energy of the gamma ray[2]. In the region of higher photon energies above approximately 100 Mev the predominant reaction results in an ejected proton which frequently possesses an energy comparable to that of the incident gamma ray. The common method of observing these higher energy reactions has been to bombard the target nuclei with high energy x-rays from bremsstrahlung sources. Because the bremsstrahlung spectrum falls off rapidly with increasing energy the strong weighting of lower energy protons makes interpretation of the observations difficult.

However, numerous observations have resulted in a large amount of information on high energy protons from x-rays on various targets. Protons of energies between 10 and 70 Mev were studied by Levinthal and Silverman[3] using the 322 Mev Berkeley synchrotron yielding a proton energy spectrum which fell off roughly as E^{-2}. While the 10 Mev protons were ejected isotropically (probably the tail of the evaporation spectra) the 40 Mev protons showed a distinct forward peaking in angular distribution. Walker[4] employed a 195 Mev x-ray beam from the Cornell synchrotron to observe protons of energies greater than about 70 Mev. He observed a forward peaking in the angular distribution and a more rapid decrease with energy of about

E^{-5} in the integral proton spectrum. Observations of protons up to energies of about 200 Mev and over wider ranges of angles and target elements were made by Keck[5] at Cornell using 300 Mev x-rays. He observed the following: the cross section for photoproton ejection increased linearly with atomic number; the angular distributions peaked more in the forward direction with increasing energy; and the proton spectra showed a sharp break in slope at an energy of approximately half of the maximum photon energy.

Levinger[6], on the basis of the last feature, developed theoretically a model in which the energetic photoprotons result from the direct interaction of the photons with neutron-proton pairs (i.e. deuteron like sub units) in the nucleus. Further confirmation for Levinger's model came from the measurements of Rosengren and Dudley[7] using 322 Mev x-rays from the Berkeley synchrotron, by Perry and Keck[8] who employed a subtraction technique to obtain the effect of monochromatic gamma rays, by Weil and McDaniel[9] using monochromatic 190 Mev gamma rays and by Feld et al[2] in this laboratory.

However, other features of the high energy photo-production distributions are not nearly as successfully accounted for by the quasi-deuteron model of Levinger[6]. In particular, the observed angular distributions appeared to be more strongly peaked in the forward direction than those predicted by the model.

Feld et al[2] observed the angular distribution of protons of 126, 169 and 203 Mev. The results differed from the predictions of Levinger's model in the positions of the maxima (if any) and the failure to observe a kinematical "cutoff". The quasi-deuteron model

E^{-5} in the integral proton spectrum. Observations of protons up to energies of about 200 Mev and over wider ranges of angles and target elements were made by Keck[5] at Cornell using 300 Mev x-rays. He observed the following: the cross section for photoproton ejection increased linearly with atomic number; the angular distributions peaked more in the forward direction with increasing energy; and the proton spectra showed a sharp break in slope at an energy of approximately half of the maximum photon energy.

Levinger[6], on the basis of the last feature, developed theoretically a model in which the energetic photoprotons result from the direct interaction of the photons with neutron-proton pairs (i.e. deuteron like sub units) in the nucleus. Further confirmation for Levinger's model came from the measurements of Rosengren and Dudley[7] using 322 Mev x-rays from the Berkeley synchrotron, by Perry and Keck[8] who employed a subtraction technique to obtain the effect of monochromatic gamma rays, by Weil and McDaniel[9] using monochromatic 190 Mev gamma rays and by Feld et al[2] in this laboratory.

However, other features of the high energy photo-production distributions are not nearly as successfully accounted for by the quasi-deuteron model of Levinger[6]. In particular, the observed angular distributions appeared to be more strongly peaked in the forward direction than those predicted by the model.

Feld et al[2] observed the angular distribution of protons of 126, 169 and 203 Mev. The results differed from the predictions of Levinger's model in the positions of the maxima (if any) and the failure to observe a kinematical "cutoff". The quasi-deuteron model

would predict pronounced maxima between 30 and 60 degrees for the energies at which the observations were made. According to Feld et al[2] the peaks (if any) were well below 30 degrees. It was pointed out by Rosengren and Dudley[7] that this does not necessarily contradict the quasi-deuteron model as Levinger assumed a $\sin^2\theta$ angular distribution in the center of mass system for the deuteron photo-disintegration. A flatter, or forward peaked deuteron cross section (which is not excluded by the existing data on the photodisintegration of the deuteron[10,11]), would be consistent with the observed high energy photoproton distributions from heavier nuclei.

The failure to observe a kinematical "cutoff" in the angular distribution can be reconciled with the quasi-deuteron model if the distributions of the nucleons within a carbon nucleus contain a very large component of nucleons with relatively higher momenta than that predicted by the Fermi distribution.

A more direct test of the quasi-deuteron model is the observance of the simultaneous emission of a neutron and a proton together with their angular correlations. Such events have been observed by Myers, Odian, Stein and Wattenberg[12] in this laboratory and by Barton and Smith[13] employing 265 Mev bremsstrahlung from the University of Illinois betatron. Substantial support for the quasi-deuteron model was provided by these observations. The neutron-proton coincidences were observed to have the kinematical relationships of a deuteron in motion*.

*For a discussion of and curves relating to the kinematics of the photo-disintegration of the deuteron see Wiener[14] who used relativistic momentum and energy conservation to calculate the energy and angular distributions.

would predict pronounced maxima between 30 and 60 degrees for the energies at which the observations were made. According to Reid et al[2] the peaks (if any) were well below 30 degrees. It was pointed out by Rosengren and Dudley[7] that this does not necessarily contradict the quasi-deuteron model as Levinger assumed a $\sin^2\theta$ angular distribution in the center of mass system for the deuteron photo-disintegration. A flatter, or forward peaked deuteron cross section (which is not excluded by the existing data on the photodisintegration of the deuteron[10,11]), would be consistent with the observed high energy photoproton distributions from heavier nuclei.

The failure to observe a kinematical "cutoff" in the angular distribution can be reconciled with the quasi-deuteron model if the distributions of the nucleons within a carbon nucleus contain a very large component of nucleons with relatively higher momenta than that predicted by the Fermi distribution.

A more direct test of the quasi-deuteron model is the observance of the simultaneous emission of a neutron and a proton together with their angular correlations. Such events have been observed by Myers, Odian, Stein and Wattenberg[12] in this laboratory and by Barton and Smith[13] employing 265 Mev bremsstrahlung from the University of Illinois betatron. Substantial support for the quasi-deuteron model was provided by these observations. The neutron-proton coincidences were observed to have the kinematical relationships of a deuteron in motion.*

*For a discussion of and curves relating to the kinematics of the photo-disintegration of the deuteron see Wiener[14] who used relativistic momentum and energy conservation to calculate the energy and angular distributions.

The results obtained showed a broader angular distribution (for fixed proton energy and angle) of neutrons about the predicted angles for heavier nuclei than for deuterium. It is manifest that this angular distribution can arise from the momenta of the nucleons within the nucleus.

Studies by Wattenberg et al (unpublished) were made in this laboratory of the widths of the neutron angular distribution as a function of energy of the photoprotons (and therefore of the photoneutron). These studies showed that the widths could be quantitatively connected with the internal momentum of the quasi-deuteron. The possibility arose of employing this effect as a tool to study the momenta of nucleons within a nucleus. In this connection a discussion of previous information on the momenta of nucleons within a nucleus is in order.

B. Momenta of Nucleons in Nuclei

Nuclear internal momenta have been studied by several observers employing different techniques; also the application of several proposed theoretical momentum distributions to experimental results has been attempted. Among the proposed momentum distributions are the statistical gas model of Fermi[15], the Chew-Goldberger[16] distribution and the gaussian distribution.

Fermi[15] employed a statistical gas model of the nucleus. The nucleus is considered to be a gas of neutrons and protons confined to a volume $\Omega = \frac{4}{3}\pi R_0^3 A$. The number of states of

The results obtained showed a broader angular distribution (for fixed proton energy and angle) of neutrons about the predicted angles for heavier nuclei than for deuterium. It is manifest that this angular distribution can arise from the moments of the nucleons within the nucleus.

Studies by Wattenberg et al (unpublished) were made in this laboratory of the widths of the neutron angular distribution as a function of energy of the photoprotons (and therefore of the photo-neutron). These studies showed that the widths could be quantitatively connected with the internal momentum of the quasi-deuteron. The possibility arose of employing this effect as a tool to study the moments of nucleons within a nucleus. In this connection a discussion of previous information on the moments of nucleons within a nucleus is in order.

B. Moments of Nucleons in Nuclei

Nuclear internal moments have been studied by several observers employing different techniques; also the application of several proposed theoretical momentum distributions to experimental results has been attempted. Among the proposed momentum distributions are the statistical gas model of Fermi[15], the Chew-Goldberger[16] distribution and the gaussian distribution.

Fermi[15] employed a statistical gas model of the nucleus. The nucleus is considered to be a gas of neutrons and protons confined to a volume $\Omega = \frac{4}{3}\pi R_0^3 A$. The number of states of

momentum, n, less than P_{max} of a proton confined to Ω is

$$n = 2\,\frac{4\pi P_{max}^3\,\Omega}{3(2\pi\hbar)^3}$$ (Factor 2 is for spin)

If the degeneracy is complete, $n = Z$; hence:

$$P_{max}^{proton} = (3\pi^2)^{\frac{1}{3}}\,\hbar\left(\frac{Z}{\Omega}\right)^{\frac{1}{3}}$$

and $N = A - Z$ for the neutrons

$$P_{max}^{neutron} = (3\pi^2)^{\frac{1}{3}}\,\hbar\left(\frac{A-Z}{\Omega}\right)^{\frac{1}{3}}$$

Making the approximation that $Z = N = \frac{A}{2} = n$

$$P_{max} = (3\pi^2)^{\frac{1}{3}}\left(\frac{A}{2\,\frac{4\pi}{3}R_o^3 A}\right)^{\frac{1}{3}}$$

This corresponds to kinetic energies in the range from 21 to 29 Mev depending on the value of R_o employed[17]. This formulation predicts that all momentum states are occupied up to this maximum and none above it.

To fit the results of observations by Hadley and York[18], Chew and Goldberger[16] postulated a momentum distribution for carbon:

$$\frac{\alpha}{\pi^2(\alpha^2+p^2)}$$

where α is a momentum corresponding to a nucleon energy of 18 Mev.

The gaussian distribution is proportional to $e^{-\frac{p^2}{2mE_g}}$

The gaussian is the same in both momentum and x space.

The usual and most obvious approach to the study of nuclear internal momenta is by observation of an interaction with a single nucleon in the nucleus. Results of these interactions are analyzed on a kinematic basis and the energy and/or angular spreads obtained are ascribed to the initial momentum of the nucleons within the nucleus. Also the deviations in threshold energies for π meson production has

momentum, n, less than P_{max} of a proton confined to Ω is

$$n = 2\,\frac{4\pi P_{max}^{3}\,\Omega}{3(2\pi\hbar)^{3}} \quad \text{(factor 2 is for spin)}$$

If the degeneracy is complete, $n = Z$; hence:

$$P_{max}^{proton} = (3\pi^{2})^{\frac{1}{3}}\,\hbar\left(\frac{Z}{\Omega}\right)^{\frac{1}{3}}$$

and $N=A-Z$ for the neutrons

$$P_{max}^{neutron} = (3\pi^{2})^{\frac{1}{3}}\,\hbar\left(\frac{A-Z}{\Omega}\right)^{\frac{1}{3}}$$

Making the approximation that $Z = N = \frac{A}{2} = n$

$$P_{max} = (3\pi^{2})^{\frac{1}{3}}\left(\frac{A}{2\,\frac{4}{3}\pi r_0^{3} A}\right)^{\frac{1}{3}}$$

This corresponds to kinetic energies in the range from 21 to 29 Mev depending on the value of r_0 employed[17]. This formulation predicts that all momentum states are occupied up to this maximum and none above it.

To fit the results of observations by Hadley and York[18], Chew and Goldberger[16] postulated a momentum distribution for nucleons:

$$\frac{\alpha}{\pi^{2}(\alpha^{2}+p^{2})^{2}}$$

where α is a momentum corresponding to a nucleon energy of 18 Mev.

The gaussian distribution is proportional to $e^{-\frac{p^{2}}{2mE_g}}$

The gaussian is the same in both momentum and x space.

The usual and most obvious approach to the study of nuclear internal momenta is by observation of an interaction with a single nucleon in the nucleus. Results of these interactions are analyzed on a kinematic basis and the energy and/or angular spreads obtained are ascribed to the initial momentum of the nucleons within the nucleus. Also the deviations in threshold energies for π meson production has

been employed to provide information on nucleon momenta.

Hadley and York[18] employed a beam of 90 Mev neutrons from the 184-in. Berkeley synchrocyclotron to produce deuterons from the bombardment of target nuclei. In this case the neutron "picks up" a partner proton from the nucleus and emerges as a deuteron. Since it is necessary for the relative momenta of the proton and the neutron to form a state of the deuteron, the process involves the momentum distribution of both the picked up proton and the deuteron. The observed distribution of deuterons for carbon was explained somewhat arbitrarily by Chew and Goldberger[16]. However, Heidman[19] was also able to fit an excited Fermi gas distribution, with a temperature corresponding to an excitation of 9 Mev, to York's data.

High energy proton-proton scattering experiments have been performed by Chamberlain and Segrè[20], Cladis[21] and Wilcox[22] using 340 Mev protons from the Berkeley 184-in. synchrocyclotron. If the struck proton is assumed to be at rest the nonrelativistic energy of the observed proton is $E_o \cos^2\theta$ (neglecting the binding energy of the proton and the excitation energy of the residual nucleus) on the basis of the two-body problem where E_o is the energy of the incident proton and θ is the angle of observation. However, the energy spectrum is smeared out due to the finite momentum of the struck proton. Chamberlain and Segrè[20] studied pairs of protons emitted in coincidence from lithium as a function of the angle between the two protons. The resulting data could be fitted with a Fermi gas momentum distribution with a maximum energy of 20 Mev.

been employed to provide information on nucleon momenta.

Hadley and York[18] employed a beam of 90 Mev neutrons from the 184-in. Berkeley synchrocyclotron to produce deuterons from the bombardment of target nuclei. In this case the neutron "picks up" a partner proton from the nucleus and emerges as a deuteron. Since it is necessary for the relative momenta of the proton and the neutron to form a state of the deuteron, the process involves the momentum distribution of both the picked up proton and the deuteron. The observed distribution of deuterons for carbon was explained somewhat arbitrarily by Chew and Goldberger[16]. However, Heidmann[19] was also able to fit an excited Fermi gas distribution with a temperature corresponding to an excitation of 9 Mev, to York's data.

High energy proton-proton scattering experiments have been performed by Chamberlain and Segrè[20], Cladis[21] and Wilcox[22] using 340 Mev protons from the Berkeley 184-in. synchrocyclotron. If the struck proton is assumed to be at rest the nonrelativistic energy of the observed proton is $E_0 \cos^2\theta$ (neglecting the binding energy of the proton and the excitation energy of the residual nucleus) on the basis of the two-body problem where E_0 is the energy of the incident proton and θ is the angle of observation. However, the energy spectrum is smeared out due to the finite momentum of the struck proton. Chamberlain and Segrè[20] studied pairs of protons emitted in coincidence from lithium as a function of the angle between the two protons. The resulting data could be fitted with a Fermi gas momentum distribution with a maximum energy of 20 Mev.

Cladis[21] observed the distribution of single protons quasi-elastically scattered from carbon at 40 degrees. The nuclear internal momentum he deduced was best fitted by a Gaussian distribution with a 1/e value of about 16 Mev.

Wilcox[22] studied by proton-proton coincidences the momentum of the protons emerging from the collisions. He observed coincidences from hydrogen, deuterium, beryllium, lithium and boron. He found the best fit to the experimental data for beryllium was a gaussian momentum distribution with a 1/e value of 20 Mev. However, any value between 15 and 25 Mev would fit the data. Fermi (rectangular) and Chew-Goldberger distributions did not fit as well. An excited Fermi distribution would fit within the accuracy of the experiment. He observed qualitative differences between lithium, beryllium and boron. He interpreted these on the basis of the proton distribution in the nucleus.

The shift in the threshold for meson production from free nucleon-nucleon production to nucleon-nucleus production has been used to examine nuclear internal momenta. The threshold energy required in the nucleon-nucleus reaction is lower than that required by the free nucleon-nucleon reaction by the energy corresponding to the momentum of the nucleon in the nucleus as predicted by McMillan and Teller[23]. Henley and Huddlestone[24] and Henley[25] have discussed the nucleonic production of π mesons in complex nuclei using several momentum distributions. The distribution employed affects the production threshold, excitation function and the energy spectrum and angular distribution of the produced mesons as compared with those resulting from collisions with

Cladis[21] observed the distribution of single protons quasi-elastically scattered from carbon at 40 degrees. The nuclear internal momentum he deduced was best fitted by a Gaussian distribution with a 1/e value of about 16 Mev.

Wilcox[22] studied by proton-proton coincidences the momentum of the protons emerging from the collisions. He observed coincidences from hydrogen, deuterium, beryllium, lithium and boron. He found the best fit to the experimental data for beryllium was a gaussian momentum distribution with a 1/e value of 20 Mev. However, any value between 15 and 25 Mev would fit the data. Fermi (rectangular) and Chew-Goldberger distributions did not fit as well. An excited Fermi distribution would fit within the accuracy of the experiment. He observed qualitative differences between lithium, beryllium and boron. He interpreted these on the basis of the proton distribution in the nucleus.

The shift in the threshold for meson production from free nucleon-nucleon production to nucleon-nucleus production has been used to examine nuclear internal momenta. The threshold energy required in the nucleon-nucleus reaction is lower than that required by the free nucleon-nucleon reaction by the energy corresponding to the momentum of the nucleon in the nucleus as predicted by McMillan and Teller[23]. Henley and Huddlestone[24] and Henley[25] have discussed the mesonic production of π mesons in complex nuclei using several momentum distributions. The distribution employed affects the production threshold, excitation function and the energy spectrum and angular distribution of the produced mesons as compared with those resulting from collisions with

free nucleons used as targets. Henley found that a gaussian distribution with a 1/e value of 19.3 Mev was the best fit to the data. He also used a 0°K Fermi degenerate gas model distribution and a modified Chew-Goldberger distribution. To eliminate the excess high momentum components and the infinite average energy in the Chew-Goldberger distribution he suggested the following modified form:

$$\frac{1}{(\alpha^2+p^2)^2(\beta^2+p^2)^2}$$

where $\beta = 2.5\,\alpha$. This has an average energy of 48.1 Mev and yet fits York's data fairly well. Block, Passman and Havens[26] have performed similar calculations for data obtained at the Columbia cyclotron with an energy of 380 Mev, at first finding the best fit given with the original Chew-Goldberger distribution, but later[27] they have used a gaussian distribution with a 1/e value of 14 Mev.

Bjorklund, Crandall, Moyer and York[28] observed high energy gamma rays resulting from the bombardment of beryllium and carbon with 340 Mev protons from the Berkeley synchrocyclotron in looking for evidence of the π^0 meson. They obtained a fit to the results on the assumption that the center of mass system was moving with $\beta = 0.32$. If the nucleon had been at rest β would have been 0.39. Because the excitation function increases with energy most of the π^0 production comes from nucleons in the target which are moving toward the beam. For $\beta = 0.32$ the energy of such a proton would be 22 Mev.

Steinberger and Bishop[29] observed the production of mesons from complex nuclei by use of the Berkeley synchrotron bremsstrahlung

free nucleons used as targets. Henley found that a gaussian distribution with a 1/e value of 15.[illegible] Mev was the best fit to the data. He also used a 0°K Fermi degenerate gas model distribution and a modified Chew-Goldberger distribution. To eliminate the excess high momentum components and the infinite average energy in the Chew-Goldberger distribution he suggested the following modified form:

$$\frac{1}{(\alpha^2+p^2)^2(\beta^2+p^2)^2}$$

where $\beta = 2.5\,\alpha$. This has an average energy of 45 Mev and gives a good fit to York's data fairly well. Block, Passman and Havens[26] have performed similar calculations for data obtained at the Columbia cyclotron with an energy of 380 Mev, at first finding the best fit given with the original Chew-Goldberger distribution, but later[27] they have used a gaussian distribution with a 1/e value of 14 Mev.

Bjorklund, Crandall, Moyer and York[28] observed high energy gamma rays resulting from the bombardment of beryllium and carbon with 340 Mev protons from the Berkeley synchrocyclotron in looking for evidence of the π^0 meson. They obtained a fit to the results on the assumption that the center of mass system was moving with $\beta = 0.$[illegible]. If the nucleon had been at rest β would have been 0.39. Because the excitation function increases with energy most of the π^0 production comes from nucleons in the target which are moving toward the beam. For $\beta = 0.32$ the energy of such a proton would be [illegible] Mev.

Steinberger and Bishop[29] observed the production of mesons from complex nuclei by use of the Berkeley synchrotron irradiating

spectrum. The meson energy and direction of production are broadened from that predicted (by a Comptonlike process) because of the bremsstrahlung spectrum and internal momentum distributions. Lax and Feshback[30] interpreted their results and found agreement with the Chew-Goldberger distribution.

It should be pointed out that it is difficult within the errors of an experiment to say which momentum distribution really fits best, and even when the type of distribution is decided upon its constants are equally difficult to determine (e.g. Wilcox[22], while he chooses 20 Mev for the 1/e value of the gaussian momentum distribution of beryllium, he finds any value from 15 to 25 Mev a satisfactory fit to the data). Table I contains a brief summary of investigations devoted primarily to nuclear internal momenta. The last column lists the distributions fitted (if any) to their results.

It is to be noted that the previous experimenters (except Wilcox[22]) have studied momentum distributions in a single nucleus. From the above work it appeared worthwhile as a first experiment to investigate whether or not nucleon momenta are the same in different nuclei. From the work of others it appears more difficult to obtain reliable detailed momentum distributions, and there is essentially no information on whether the momentum distributions obtained were specific to the element being studied.

This thesis describes the use of the quasi-deuteron for an experimental study of relative internal momenta. As such the experimental techniques and observations are refinements and extensions to more angles

spectrum. The meson energy and direction of production are unaltered from that predicted (by a Comptonlike process) because of the bremsstrahlung spectrum and internal momentum distributions. Lax and Feshbach[30] interpreted their results and found agreement with the Chew-Goldberger distribution.

It should be pointed out that it is difficult within the errors of an experiment to say which momentum distribution really fits best, and even when the type of distribution is decided upon its constants are equally difficult to determine (e.g., Wilcox[22], while he chooses 20 Mev for the 1/e value of the gaussian momentum distribution of beryllium, he finds any value from 15 to 25 Mev a satisfactory fit to the data). Table I contains a brief summary of investigations devoted primarily to nuclear internal momenta. The last column lists the distributions fitted (if any) to their results.

It is to be noted that the previous experimenters (except Wilcox[22]) have studied momentum distributions in a single nucleus. From the above work it appeared worthwhile as a first experiment to investigate whether or not nucleon momenta are the same in different nuclei. From the work of others it appears more difficult to obtain reliable detailed momentum distributions, and there is essentially no information on whether the momentum distributions obtained were specific to the element being studied.

This thesis describes the use of the quasi-deuteron for an experimental study of relative internal momenta. As such the experimental techniques and observations are refinements and extensions to more angles

TABLE I

Summary of Other Investigations of Nucleon Momenta

Author and Reference	Technique	Element	Distribution Applied
Hadley and York[18]	Proton-pickup by neutrons	C	Normal Chew-Goldberger[16]
Chamberlain and Segrè[20]	Angle between protons in P-P scattering	Li	Fermi[15] distribution with maximum energy of 20 Mev
Cladis[21]	"Quasi-elastic" P-P scattering	C	Gaussian with 1/e value of 16 Mev
Wilcox[22]	Momentum analysis of one of the protons from P-P scattering coincidences	Li	None
		Be	Gaussian with 1/e value of 20 Mev
		B	None

TABLE I

Summary of Other Investigations of Nucleon Momenta

Author and Reference	Technique	Element	Distribution Applied
Hedley and York[18]	Proton-pickup by neutrons	C	Normal Chew-Goldberger[16]
Chamberlain and Segrè[20]	Angle between protons in P-P scattering	Li	Fermi[15] distribution with maximum energy of 20 Mev
Cladis[21]	"Quasi-elastic" P-P scattering	C	Gaussian with 1/e value of 16 Mev
Wilcox[22]	Momentum analysis of one of the protons from P-P scattering coincidences	Li	None
		Be	Gaussian with 1/e value of 20 Mev
		B	None

and more nuclei of the previous works in this laboratory[2,12]. As a part of this work it has been necessary to understand the efficiency and angular resolution of the neutron detector employed. This phase of the work has been described separately by Christie[31].

II. Experimental Equipment

A. Accelerator and Monitor

This experiment was performed with a 340 Mev bremsstrahlung beam from the M.I.T. synchrotron. The synchrotron has a repetition rate of six pulses per second. During each pulse the beam has a duration of about 1200 microseconds.

The monitor employed was of the ionization chamber type. For a description of the calibration of this monitor see Odian[32] and Ratz[33]. The unit of measure of the monitor was referred to as a "mouse". In this experiment the "mouse" corresponded to about 0.6×10^8 "equivalent quanta". The number of "equivalent quanta" is the total energy in a photon beam divided by the maximum photon energy.

The general arrangement of the experimental equipment is shown in Figure 1. The various components are described below.

B. Counter Telescopes

The method of proton detection employed was of essentially the same type employed in previous investigations in this laboratory[2]. A two crystal scintillation counter was employed to detect a fairly monoenergetic group of protons and to distinguish them from other charged particles by means of pulse height observation. The crystals employed were of Pilot "B" plastic. The front crystal was $\frac{1}{2}$ inch thick and the back crystal was 2 inches thick. Both crystals were 5 inches in diameter and were mounted in a Lucite frame as shown in Figure 2.

II. Experimental Equipment

A. Accelerator and Monitor

This experiment was performed with a 340 Mev bremsstrahlung beam from the M.I.T. synchrotron. The synchrotron has a repetition rate of six pulses per second. During each pulse the beam has a duration of about 1200 microseconds.

The monitor employed was of the ionization chamber type. For a description of the calibration of this monitor see Odian[32] and Rate[33]. The unit of measure of the monitor was referred to as a "mouse". In this experiment the "mouse" corresponded to about 0.6×10^{8} "equivalent quanta". The number of "equivalent quanta" is the total energy in a photon beam divided by the maximum photon energy.

The general arrangement of the experimental equipment is shown in Figure 1. The various components are described below.

B. Counter Telescope

The method of proton detection employed was of essentially the same type employed in previous investigations in this laboratory[2]. A two crystal scintillation counter was employed to detect a fairly monoenergetic group of protons and to distinguish them from other charged particles by means of pulse height observation. The crystals employed were of Pilot "B" plastic. The front crystal was 1/4 inch thick and the back crystal was 2 inches thick. Both crystals were [illegible] inches in diameter and were mounted in a Lucite frame as shown in Figure [illegible].

Figure 1

General Arrangement of Experimental Equipment
(not to scale)

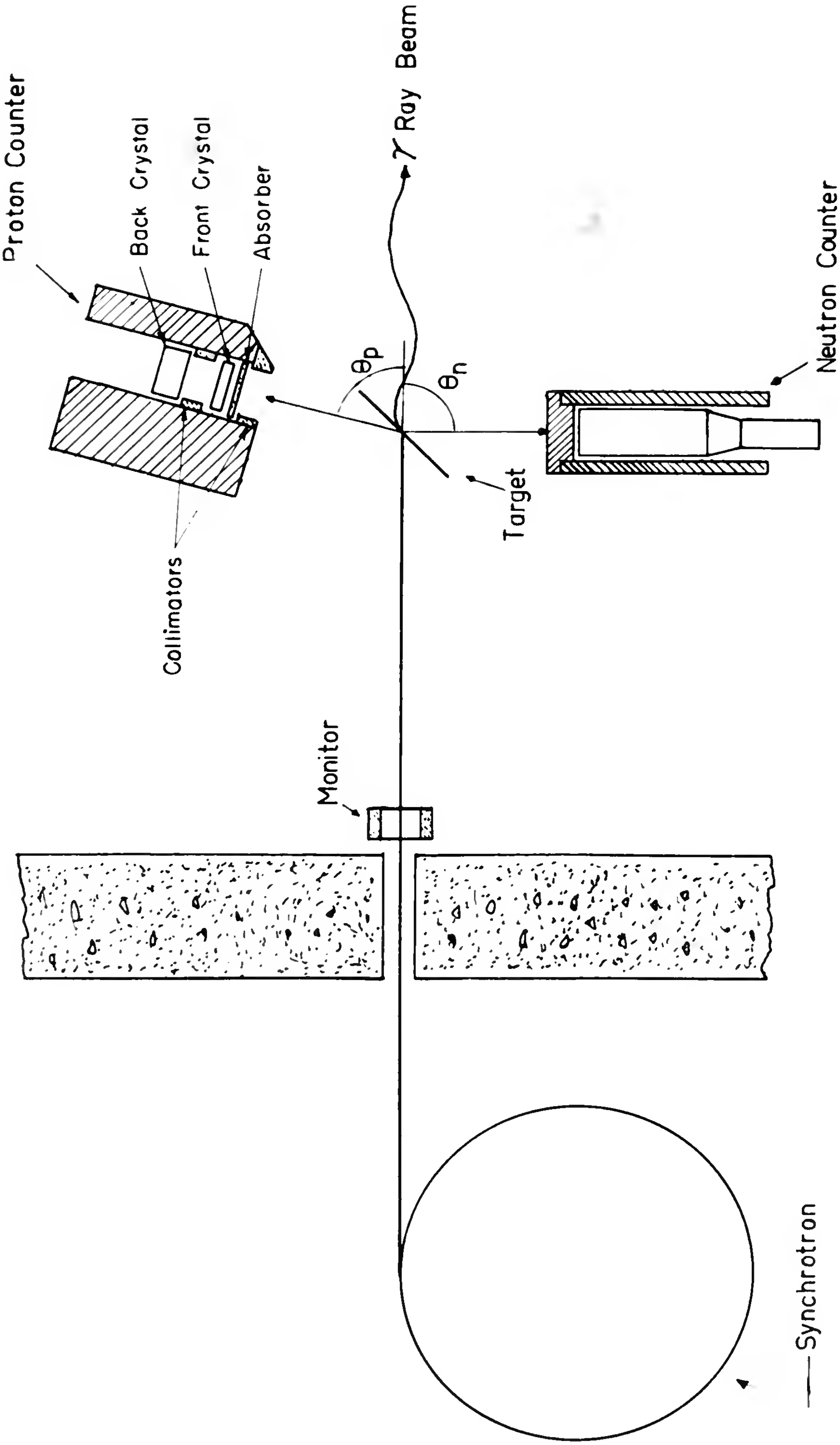
Proton Counter
Back Crystal
Front Crystal
Absorber
γ Ray Beam
θp
θn
Neutron Counter
Target
Collimators
Monitor
Synchrotron

Figure 1

Figure 2

Details of Proton Detector Lucite Frame

Figure 2

Details of Proton Detector Lucite Frame

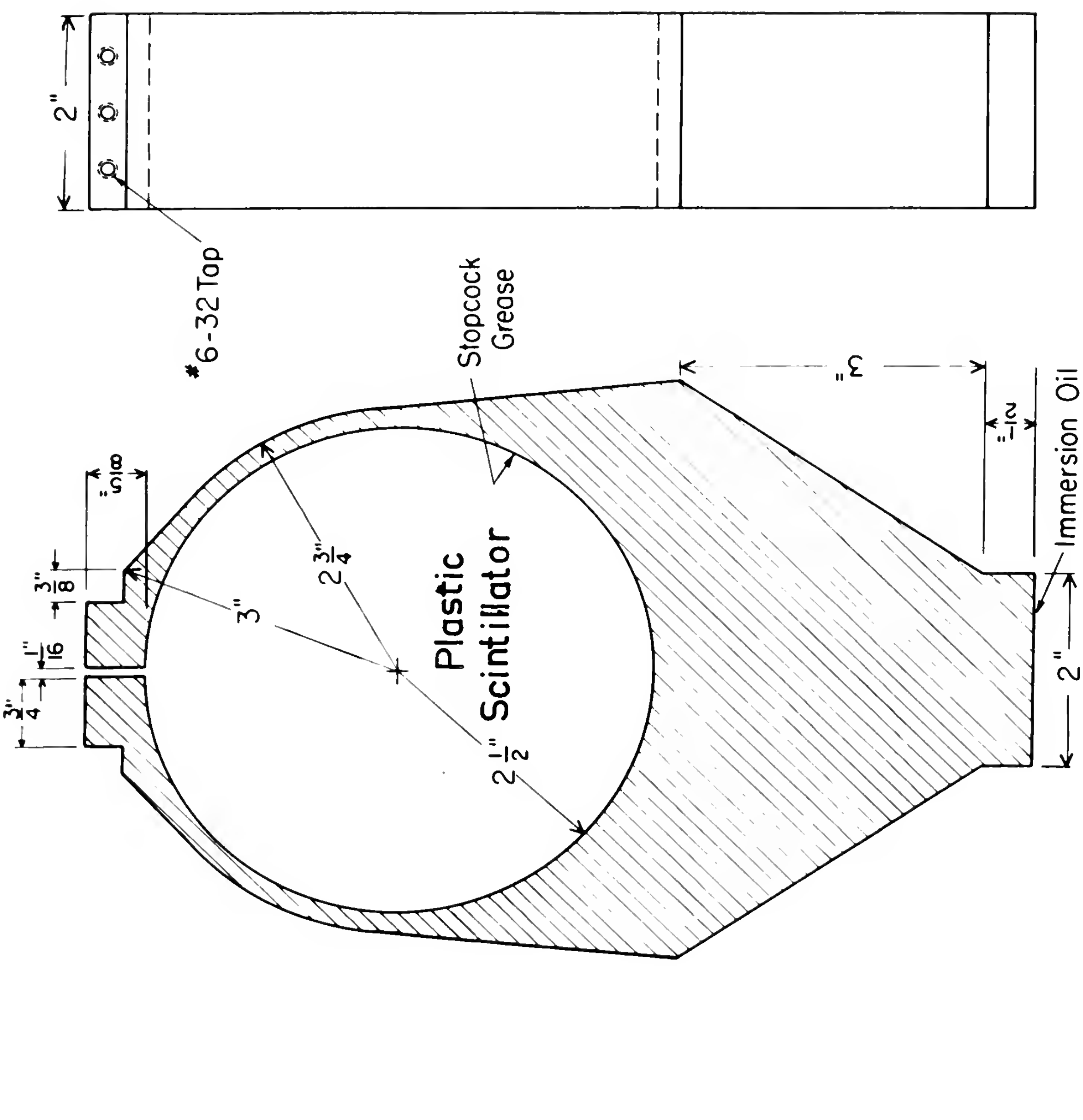
2"
#6-32 Tap
Stopcock Grease
Plastic Scintillator
Immersion Oil
3"
2"

Figure 2

End window (5819) photomultipliers were placed in optical contact with the Lucite frame at a distance of 4 inches from the crystal edge in order to increase the uniformity of the light collection from the crystal. A 0.375 inch brass absorber was placed in front of the front crystal in order to obtain the proper energy group and pulse height relationship in the back crystal. This arrangement corresponded to observing protons with energies from 117 to 142 Mev. Two brass collimators of four inches diameter were also inserted in the telescope. The arrangement of these components may be seen in Figure 1. The energies observed correspond to the peak of the back crystal pulse height curve as shown in Figure 3. For a complete description of the calibration of ΔE for this counter see Odian[32].

The neutron counter consisted of an annealed Lucite cylinder four inches in diameter and 12 inches long as shown in Figure 4. It was filled with a scintillating liquid composed of cyclohexylbenzene with 30 grams of p-terphenyl per liter added. A 5819 photomultiplier tube viewed it from the rear. The side was surrounded by a lead cylinder 1-1/8 inches thick. The face of the counter was behind a two inch lead disk to reduce the entrance of gamma rays and charged particles. A complete description and evaluation of this counter has been furnished by Christie[31].

C. Electronics

A block diagram of the electronics is shown in Figure 5. Four amplifier channels were employed. Discriminators and attenuators were

End window (5819) photomultipliers were placed in optical contact with the Lucite frame at a distance of 4 inches from the crystal edge in order to increase the uniformity of the light collection from the crystal. A 0.375 inch brass absorber was placed in front of the front crystal in order to obtain the proper energy group and pulse height relationship in the back crystal. This arrangement corresponded to observing protons with energies from 117 to 142 Mev. Two brass collimators of four inches diameter were also inserted in the telescope. The arrangement of these components may be seen in Figure 1. The energies observed correspond to the peak of the back crystal pulse height curve as shown in Figure 3. For a complete description of the calibration of ΔE for this counter see Odian[32].

The neutron counter consisted of an annealed Lucite cylinder four inches in diameter and 12 inches long as shown in Figure 4. It was filled with a scintillating liquid composed of cyclohexylbenzene with 30 grams of p-terphenyl per liter added. A 5819 photomultiplier tube viewed it from the rear. The side was surrounded by a lead cylinder 1-1/8 inches thick. The face of the counter was behind a two inch lead disk to reduce the entrance of gamma rays and charged particles. A complete description and evaluation of this counter has been furnished by Christie[31].

C. Electronics

A block diagram of the electronics is shown in Figure 5. Four amplifier channels were employed. Discriminators and attenuators were

Figure 3

Pulse Height versus Proton Energy Curves for Proton Telescope Crystals

The protons detected corresponded to pulse heights on the back (second) counter above the bias level indicated. Third counter was not used in this experiment.

Figure 3

Pulse Height versus Proton Energy Curves for Proton Telescope Crystals

The protons detected corresponded to pulse heights on the back (second) counter above the bias level indicated. Third counter was not used in this experiment.

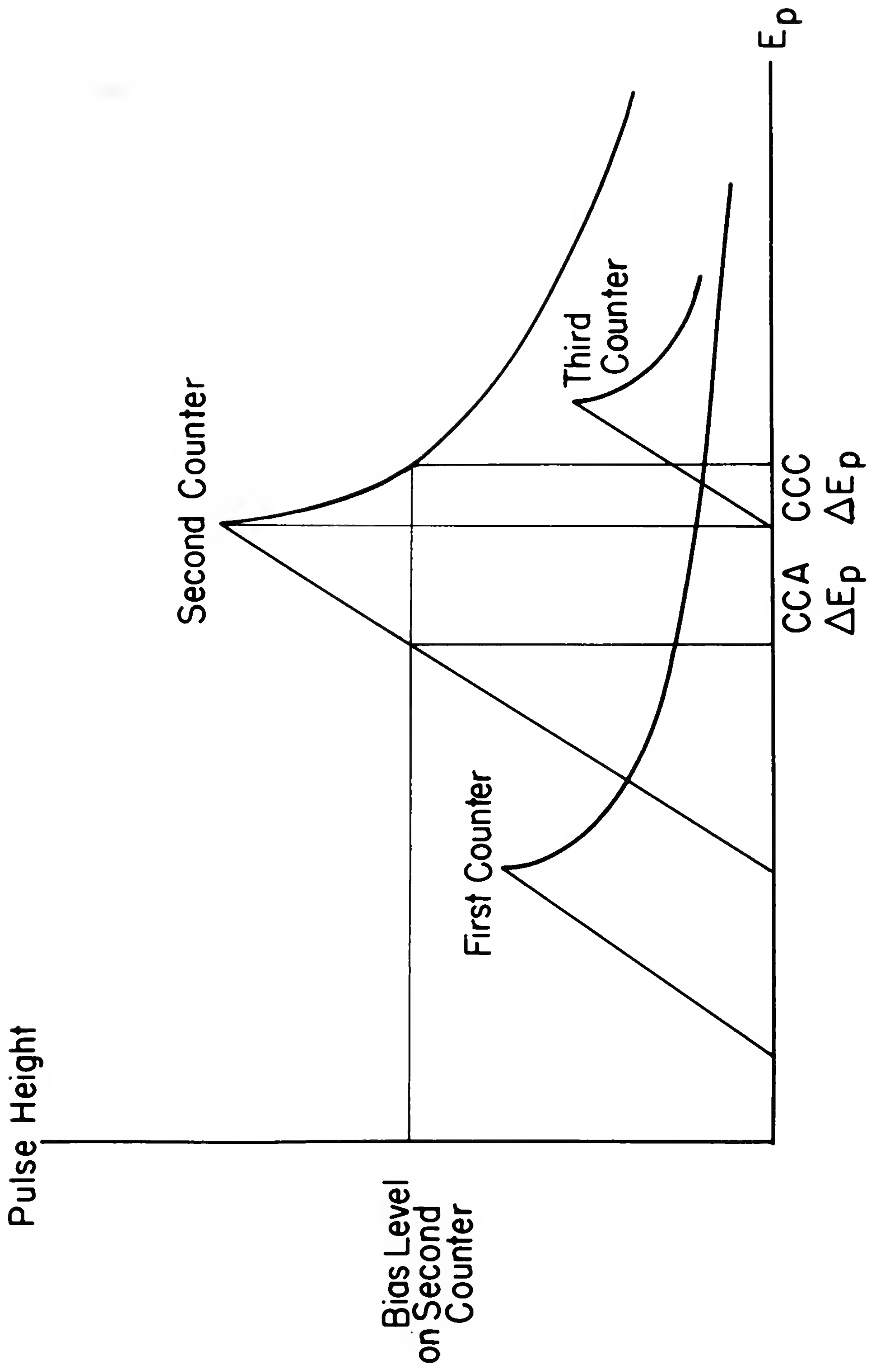
Pulse Height
Bias Level on Second Counter
First Counter
Second Counter
Third Counter
CCA
ΔE_p
CCC
ΔE_p
E_p

Figure 3

Figure 4

Details of Neutron Detector

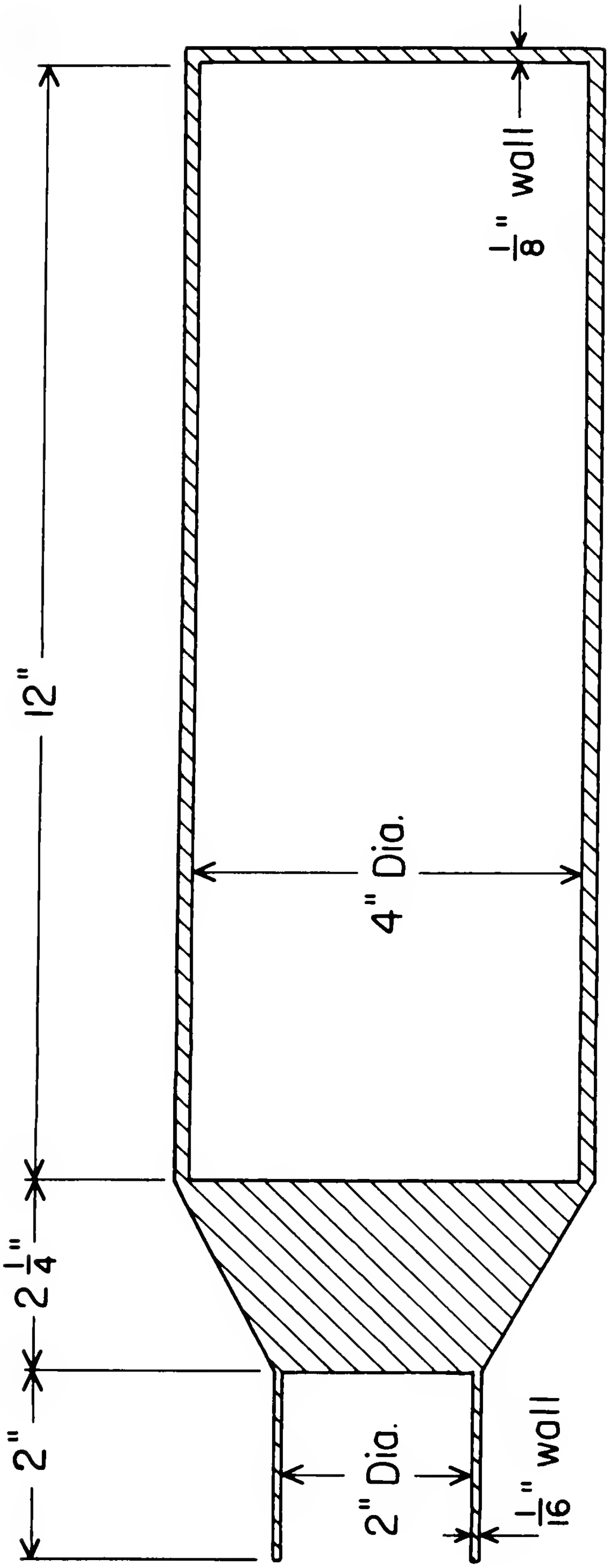

Figure 4

Figure 5

Electronics Block Diagram

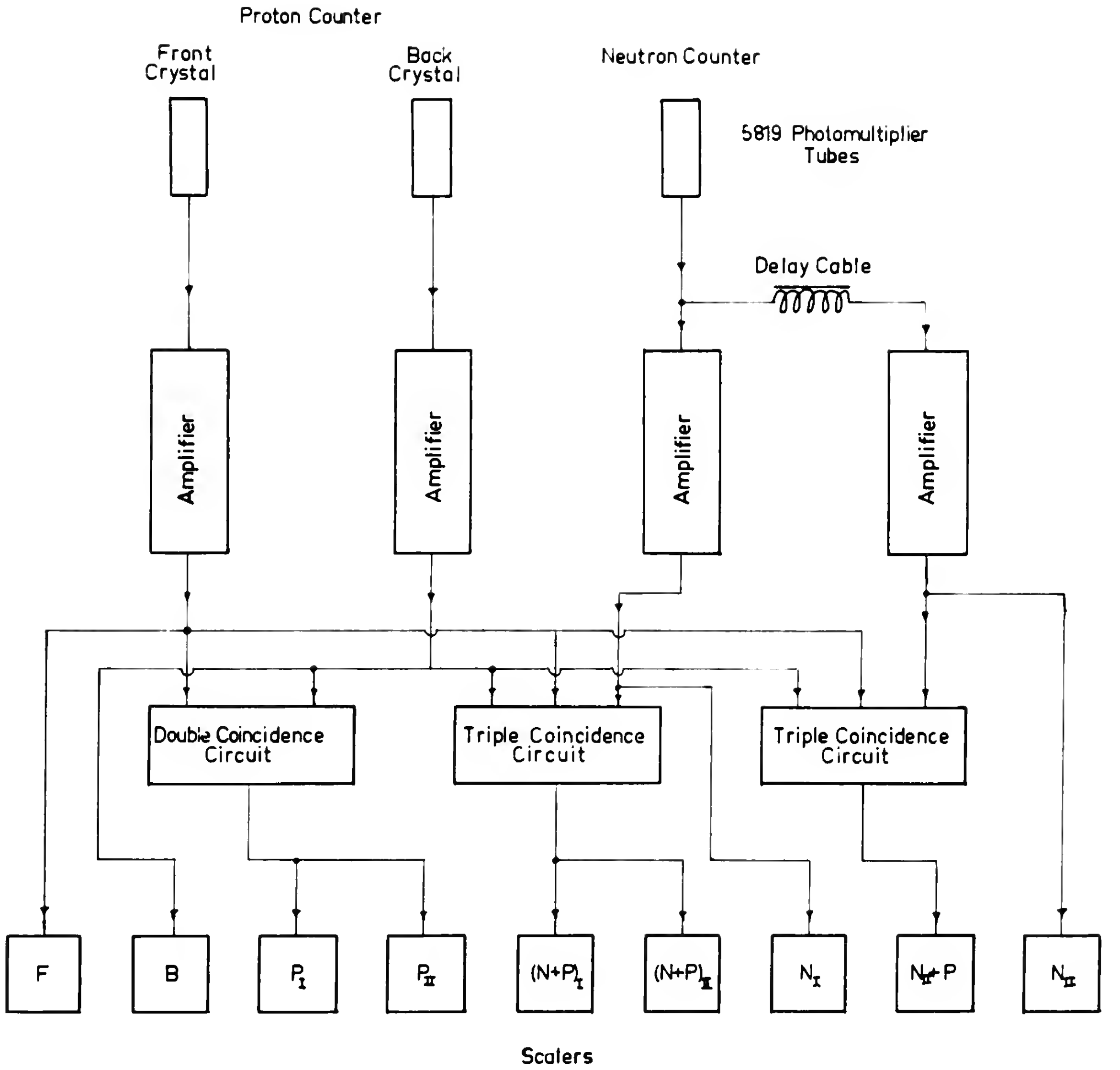
Proton Counter
Front Crystal
Back Crystal
Neutron Counter
5819 Photomultiplier Tubes
Delay Cable
Amplifier
Amplifier
Amplifier
Amplifier
Double Coincidence Circuit
Triple Coincidence Circuit
Triple Coincidence Circuit
F
B
P_I
P_{II}
$(N+P)_I$
$(N+P)_{II}$
N_I
$N_{II}+P$
N_{II}
Scalers

Figure 5

employed on the amplifiers to select the pulse height to be observed. The channels for the front and back crystals of the proton telescope are connected through a (two-fold) coincidence circuit to give the proton count. The neutron signals were sent to the regular neutron channel ($Neutrons_I$) and also through a 56 meter (0.3 microsecond) RG-63/U cable to another amplifier channel ($Neutrons_{II}$) for measuring the accidental counting rate. Each of these neutron channels was connected to a separate triple coincidence circuit with the front and back crystals of the proton counter. This arrangement gave the total neutron-proton coincidence rate and simultaneously the accidental neutron-proton coincidence rate. As a check two scalers were employed on the proton and the neutron-proton coincidence channels. The resolving time, 2τ, of the coincidence circuits was about 0.17 microseconds.

D. Targets

The targets employed in this work were water, heavy water, lithium, carbon, aluminum and copper. A description of the targets is found in Table II. It was desired to have targets of exactly the same energy loss for 130 Mev protons (i.e. ΔE = 20 Mev). However, time limitations compelled the use of the targets at hand with the result that this condition was not always realized. The energy losses for targets perpendicular to the proton counter are listed in column 5 of table II.

A special lithium metal target was cast in a dry box under a helium atmosphere. Due to uneven contraction on cooling it had to

employed on the amplifiers to select the pulse height to be observed. The channels for the front and back crystals of the proton telescope are connected through a (two-fold) coincidence circuit to give the proton count. The neutron signals were sent to the regular neutron channel (Neutrons$_{I}$) and also through a 56 meter (0.3 microsecond) RG-63/U cable to another amplifier channel (Neutrons$_{II}$) for measuring the accidental counting rate. Each of these neutron channels was connected to a separate triple coincidence circuit with the front and back crystals of the proton counter. This arrangement gave the total neutron-proton coincidence rate and simultaneously the accidental neutron-proton coincidence rate. As a check two scalers were employed on the proton and the neutron-proton coincidence channels. The resolving time, 2τ, of the coincidence circuits was about 0.17 microseconds.

D. Targets

The targets employed in this work were water, heavy water, lithium, carbon, aluminum and copper. A description of the targets is found in Table II. It was desired to have targets of exactly the same energy loss for 130 Mev protons (i.e. ΔE = 20 Mev). However, time limitations compelled the use of the targets at hand with the result that this condition was not always realized. The energy losses for targets perpendicular to the proton counter are listed in column 5 of table II.

A special lithium metal target was cast in a dry box under a helium atmosphere. Due to uneven contraction on cooling it had to

TABLE II

Target Data

Substance	Z	A	Target Thickness m/cm^2	Energy Loss(ΔE) for 130 Mev protons(Mev)	Target Angle		
					θ_N' *	θ_T for $\theta_N < \theta_N'$	θ_T for $\theta_N > \theta_N'$
Lithium	3	6.94	1.90	10.5	100	134	63
Carbon	6	12.01	3.10	18.0	96	140	50
Light Water			2.18	17		140	Not run above 100
Heavy Water			2.35	19		140	
Aluminum	13	26.98	3.35	17.2	100	140	50
Copper	29	63.54	4.38	19.2	96	140	50

*θ_N' is the neutron counter angle at which the target angle is shifted.

TABLE II

Target Data

Substance	Z	A	Target Thickness g/cm^2	Energy Loss (ΔE) for 130 Mev protons (Mev)	Target Angle θ'_N *	Target Angle θ_T for $\theta_N \leq \theta'_N$	Target Angle θ_T for $\theta_N > \theta'_N$
Lithium	3	6.94	1.90	10.5	100	134	63
Carbon	6	12.01	3.10	18.0	95	140	70
Light Water			2.18	17		140	Not run above 100
Heavy Water			2.35	19		140	
Aluminum	13	26.98	3.35	17.2	100	140	50
Copper	29	63.54	4.38	19.2	96	140	50

*θ'_N is the neutron counter angle at which the target angle is shifted.

be machined to a thickness thinner than that anticipated in order to obtain a uniform surface. It was wrapped in thin aluminum foil, and the seams were dipped in paraffin.

The heavy water and light water targets were in thin walled plastic cells. Unfortunately the tension was different in the walls of the two cells. This led to the H_2O cell being 2 percent thicker than the D_2O cell. The other samples were bare metal plates. All targets were larger than the beam.

In general targets were set at about 140 degrees to the beam. In order to keep the neutron scattering negligible in the target, the target angle was shifted to about 40 degrees when the neutron counter was at angles larger than about 100 degrees.

As pointed out in Christie's[31] analysis of the deuterium data, the finite size of the target adds to the angular resolution associated with the geometry. It was desired to keep the angular resolution the same for the various elements. A graphical analysis was made of the projection (on a perpendicular to the axis of the proton telescope) of the beam's intersection with the target. This was a function of the thickness of the target. The criterion chosen was that the proton telescope should observe a three inch projection of the portion of the target in the beam.

The angles used for the various targets are listed in the last columns of Table II. The sixth column lists the neutron counter angle at which the target angle was shifted. These angles were set

be machined to a thickness thinner than that anticipated in order to obtain a uniform surface. It was wrapped in thin aluminum foil, and the seams were dipped in paraffin.

The heavy water and light water targets were in thin walled plastic cells. Unfortunately the tension was different in the walls of the two cells. This led to the H_2O cell being 2 percent thicker than the D_2O cell. The other samples were bare metal plates. All targets were larger than the beam.

In general targets were set at about 140 degrees to the beam. In order to keep the neutron scattering negligible in the target, the target angle was shifted to about 40 degrees when the neutron counter was at angles larger than about 100 degrees.

As pointed out in Christie's[31] analysis of the deuterium data, the finite size of the target adds to the angular resolution associated with the geometry. It was desired to keep the angular resolution the same for the various elements. A graphical analysis was made of the projection (on a perpendicular to the axis of the proton telescope) of the beam's intersection with the target. This was a function of the thickness of the target. The criterion chosen was that the proton telescope should observe a three inch projection of the portion of the target in the beam.

The angles used for the various targets are listed in the last columns of Table II. The sixth column lists the neutron counter angle at which the target angle was shifted. These angles were set

within about one degree on a protractor that was centered in the beam. The protractor was centered by means of x-ray photographs of the beam.

within about one degree on a protractor that was centered in the beam. The protractor was centered by means of x-ray photographs of the beam.

III Experimental Procedure

A. Standards

Radioactive sources were employed as standards in order to minimize drift of the high voltage supplies and other electronic components. On the proton telescope the brass absorber was removed and the 500 microcurie radium source was suspended at the center of the target side of the front collimator opening. The counting rates of both the front and back crystals were observed. The neutron counter was standardized by inserting a 2 microcurie cobalt-60 source inside the cylindrical lead shield to the mid-point of the counter, and reading the counting rate on the normal neutron channel (Neutrons_I). Adjustments were made by varying the high voltage on the photomultiplier tubes. All discriminator bias settings on the amplifiers were fixed with a potentiometer. Voltage readings were made with an electrostatic voltmeter.

B. Treatment of Accidentals

As previously mentioned an evaluation of the number of accidental neutron-proton coincidences was made by employing a delayed neutron channel in coincidence with the front and back channels of the proton counter. The delayed neutron channel (Neutrons_{II}) was generally run at a lower bias and hence higher counting rate than the normal neutron channel (Neutrons_I) to obtain better statistics. The accidental neutron-proton counts were normalized to the normal neutron-

III Experimental Procedure

A. Standards

Radioactive sources were employed as standards in order to minimize drift of the high voltage supplies and other electronic components. On the proton telescope the brass absorber was removed and the 500 microcurie radium source was suspended at the center of the target side of the front collimator opening. The counting rates of both the front and back crystals were observed. The neutron counter was standardized by inserting a 2 microcurie cobalt-60 source inside the cylindrical lead shield to the mid-point of the counter, and reading the counting rate on the normal neutron channel ($Neutrons_I$). Adjustments were made by varying the high voltage on the photomultiplier tubes. All discriminator bias settings on the amplifiers were fixed with a potentiometer. Voltage readings were made with an electrostatic voltmeter.

B. Treatment of Accidentals

As previously mentioned an evaluation of the number of accidental neutron-proton coincidences was made by employing a delayed neutron channel in coincidence with the front and back channels of the proton counter. The delayed neutron channel ($Neutrons_{II}$) was generally run at a lower bias and hence higher counting rate than the normal neutron channel ($Neutrons_I$) to obtain better statistics. The accidental neutron-proton counts were normalized to the normal neutrons

proton counts by the following proportion:

$$\frac{(N_{II}+P)_{normalized}}{N_{II}+P} = \frac{N_I}{N_{II}}$$

The normalized accidental counts were then subtracted from the total neutron-proton counts to give the true number of neutron-proton coincidences for the run.

C. Kinematics

Employing relativistic momentum and energy conservation the proton counter energy and angle were set so as to make the proton angle 90 degrees in the center of mass coordinates of the deuteron[14]. For 130 Mev protons this angle in the laboratory was 76 degrees. This meant the neutron angle in center of mass coordinates was 90 degrees with the consequence that it would also be 76 degrees in the laboratory. However, due to the finite size of the target and orientation relative to the two counters the peak of the neutron angular distribution should occur at a slightly larger angle as shown by Christie[31]. The observed peak of the neutron angular distribution occurred at 78 degrees in the laboratory coordinates.

D. Description of Runs

Runs were normally made first at a (protractor) setting of 78 degrees for the neutron counter. This was followed by a run on either side for the "wings" of the neutron angular distribution, and then by runs at ten degree increments to establish the shape of the distribution. One or more subsequent runs were made at 78 degrees as a check on

proton counts by the following proportion:

$$\frac{(N_{II+P})_{normalized}}{N_{I+P}} = \frac{N_{II}}{N_{I}}$$

The normalized accidental counts were then subtracted from the total neutron-proton counts to give the true number of neutron-proton coincidences for the run.

C. Kinematics

Employing relativistic momentum and energy conservation the proton counter energy and angle were set so as to make the proton angle 90 degrees in the center of mass coordinates of the deuteron[14]. For 130 Mev protons this angle in the laboratory was 76 degrees. This meant the neutron angle in center of mass coordinates was 90 degrees with the consequence that it would also be 76 degrees in the laboratory. However, due to the finite size of the target and orientation relative to the two counters the peak of the neutron angular distribution should occur at a slightly larger angle as shown by Christie[31]. The observed peak of the neutron angular distribution occurred at 78 degrees in the laboratory coordinates.

D. Description of Runs

Runs were normally made first at a (protractor) setting of 78 degrees for the neutron counter. This was followed by a run on either side for the "wings" of the neutron angular distribution, and then by runs at ten degrees increments to establish the shape of the distribution. One or more subsequent runs were made at 78 degrees as a check on

operations. Runs were made for the equivalent of 2000 normal "mice"*.

*Due to different collimations of the bremsstrahlung beam the absolute value of the "mouse" was changed several times (see description of monitor in Section IIA). It should be pointed out that the proton count and not the number of "mice" was used as the normalizing factor for plotting data.

operations. Sums were made for the equivalent of 200 normal "mice"*.

*Due to different collimations of the bremsstrahlung beam the absolute value of the "mouse" was changed several times (see description of monitor in Section IIA). It should be pointed out that the proton count and not the number of "mice" was used as the normalizing factor for plotting data.

IV. Analysis of Data

A. Reduction of Raw Data

A typical set of readings is shown in Table III to illustrate the information recorded in each run. Each count reading was divided by the number of "mice"* as a check on reproducibility. Summary tables of the data for each element were made up. The more important parts of these are reproduced in Tables IVa through IVf. These tables show the actual total counts observed and are not normalized for the number of "mice" in each run. The last column of each table gives the corrected coincidence counts divided by the proton count. Ideally the proton count should have been a constant. By dividing by the proton rate, we are correcting for the necessary changes in target position, drifts in the proton counter, drifts in the machine energy and intensity, errors in the placement of the target, errors in the monitoring system and variations in the number of "mice" per run. The values of the $\frac{N+P}{P}$ ratios were generally almost always reproducible within statistics when the points were rerun.

B. Deuterium

The neutron-proton coincidences in heavy water are assumed to be due to both the deuterium and the oxygen while those from light water are due only to the oxygen. A subtraction performed according to the following formula gave the desired values for deuterium:

$$\frac{(N+P)_{D_2O} - 0.98\,(N+P)_{H_2O}}{\text{Pave}_{\,D_2O} - 0.98\,\text{Pave}_{\,H_2O}}$$

*See Section IIID.

IV. Analysis of Data

A. Reduction of Raw Data

A typical set of readings is shown in Table III to illustrate the information recorded in each run. Each count reading was divided by the number of "mices"* as a check on reproducibility. Summary tables of the data for each element were made up. The more important parts of these are reproduced in Tables IVa through IVf. These tables show the actual total counts observed and are not normalized for the number of "mices" in each run. The last column of each table gives the corrected coincidence counts divided by the proton count. Ideally the proton count should have been a constant. By dividing by the proton rate, we are correcting for the necessary changes in target position, drifts in the proton counter, drifts in the machine energy and intensity, errors in the placement of the target, errors in the monitoring system and variations in the number of "mices" per run. The values of the $\frac{N+P}{P}$ ratios were generally almost always reproducible within statistics when the points were rerun.

B. Deuterium

The neutron-proton coincidences in heavy water are assumed to be due to both the deuterium and the oxygen while those from light water are due only to the oxygen. A subtraction performed according to the following formula gave the desired values for deuterium:

$$\frac{(N+P)_{D_2O} - 0.98\,(N+P)_{H_2O}}{P_{ave\,D_2O} - 0.98\,P_{ave\,H_2O}}$$

*See Section IIID.

TABLE III

Samples of Data Recorded During Runs

Mice*	Target	Counter Angles		Target Angle (θ_T)	Front Channel Clicks# (F)	Back Channel Count# (B)	Proton Counts#		Neutron Clicks#		Neutron-Proton Coincidence Counts#		
											Total		
		Proton (θ_P)	Neutron (θ_N)				Scaler I (P_I)	Scaler II (P_{II})	Normal (N_I)	Delayed (N_{II})	Scaler I $(N+P)_I$	Scaler II $(N+P)_{II}$	Delayed $(N_{II}+P)$
1500	C	76	88	140	0686 0026 660	6333^{12} 6159 11148	839^{9} 717 7753	160^{7} 040 7687	3849 3425 424	3656 3166 490	72^{22} 72 22	00^{22} 00 22	61^{8} 61 8
	Counts/mouse				0.440	7.44	5.17	5.13	0.283	0.327	0.0147	0.0147	0.0053
3000	C	76	88	140	1336 0026 1310	6507^{53} 6159 22325	959^{31} 717 15519	280^{25} 040 15385	4257 3425 832	5782 3166 2616	72^{48} 72 48	00^{48} 00 48	61^{9} 61 9
	Counts/mouse				0.437	7.44	5.18	5.13	0.277	0.872	0.016	0.016	0.003
1500	C	76	108	50	1887 1336 551	6653^{45} 6508 9325	061^{7} 959 6535	381^{39} 280 6503	4607 4337 270	7481 5788 1693	73^{7} 73 7	00^{7} 00 7	61^{4} 61 4
	Counts/mouse				0.367	6.22	4.36	4.33	0.180	1.13	0.0047	0.0047	0.0027
3000	C	76	108	50	2421 1336 1085	6797^{3} 6508 18499	160^{32} 959 12926	480^{59} 280 12859	4866 4337 529	9105 5188 3317	73^{15} 73 15	00^{15} 00 15	61^{6} 61 6
	Counts/mouse				0.362	6.17	4.31	4.29	0.176	1.11	0.005	0.005	0.002

* See Section III D

\# Scale of 64 scalers were used. When counting rates sufficiently high only the number of clicks was recorded. 1 click = 64 counts.

Runs were generally stopped in the middle and readings taken as a check on reproducibility

TABLE IVa

Summary of Heavy Water Data

Neutron Counter Angle (θ_N)	Proton Counts (P_I)	Neutron - Proton Coincidences		
		Total (N+P)	Corrected@	Normalized# Corrected
63	12224	37	29.6	24 ± 5
68	12180	68	62.5	51 ± 7
73	12610	127	121.2	96 ± 9
78	12235	132	126.7	103 ± 10
78	12669	146	140.2	111 ± 10
*78	24904	278	266.8	107 ± 7
83	12600	79.5	76.1	60 ± 7
83	13546	93	87.7	65 ± 7
*83	26146	172.5	163.8	63 ± 5
88	12245	47	43.5	36 ± 6
88	12821	43	37.7	29 ± 5
*88	25066	90	81.1	32 ± 4
Ave	12570			

@ Corrected Neutron-Proton Coincidences = $(N+P) - (N_{II}+P)\dfrac{N_I}{N_{II}}$

Normalized corrected neutron-proton coincidences = $\dfrac{1}{P_I}$ X Corrected Coincidences

* Combination of runs above at same angle

Taken with proton counter at 76 ± 5 degrees and with proton energy of 130 ± 12 Mev.

See Table II for data on Target

TABLE IVb

Summary of Lithium Data

Neutron Counter Angle (θ_N)	Proton Counts (P_I)	Neutron - Proton Coincidences		
		Total (N+P)	Corrected@	Normalized# Corrected
38	4505	3	1.6	4± 5
48	6829	6	4.7	7± 4
58	6798	26	26	38± 8
68	4516	45	40.9	91± 16
78	4476	49	47.6	106± 16
78	3344	27	25.6	77± 16
78	3960	32	30.7	78± 15
*78	11780	108	103.9	88± 9
88	6407	34	28.6	45± 10
98	8187	24	24	29± 6
108	7471	8	8	11± 4
118	3958	2	0.5	1± 5

@ Corrected Neutron-Proton Coincidences $= (N + P) - (N_{II} + P)\dfrac{N_I}{N_{II}}$

Normalized corrected neutron-proton coincidences $= \dfrac{1}{P_I} \times$ Corrected Coincidences

* Combination of runs above at same angle

Taken with proton counter at 76 ± 5 degrees and with proton energy of 130 ± 12 Mev.

See Table II for data on Target

TABLE XVb

Summary of Lithium Data

Neutron Counter Angle (θ_N)	Proton Counts (P_I)	Neutron – Proton Coincidences: Total (NP)	Corrected @	Normalized Corrected #
38	4505	3	1.6	4 ± 5
48	6829	6	4.7	7 ± 4
58	6798	26	26	38 ± 2
68	4516	45	40.9	91 ± 16
78	4476	49	47.6	106 ± 16
74	3344	27	25.6	77 ± 16
76	3960	32	30.7	78 ± 15
*76	11780	108	103.9	89 ± 9
88	6407	34	28.6	45 ± 10
98	8187	31	24	29 ± 6
108	7471	8	8	11 ± 4
118	3958	2	0.5	1 ± 5

@ Corrected Neutron-Proton Coincidences = $(N\,P) - (N_{II}\,P)\dfrac{N_I}{N_{II}}$

Normalized corrected neutron-proton coincidences = $\dfrac{1}{P_I}$ × Corrected coincidences

* Combination of runs above at same angle

Taken with proton counter at 76 ± 5 degrees and with proton energy of 130 ± 12 Mev.

See Table II for data on Target

TABLE IVc

Summary of Carbon Data

Neutron Counter Angle (θ_N)	Proton Counts (P_I)	Neutron - Proton Coincidences		
		Total (N+P)	Corrected@	Normalized# Corrected
38	13248	14	8.4	6.3 ± 2.9
48	8020	9	8.0	10 ± 4
58	13785	30	26.1	19 ± 4
68	13684	43	38.9	28 ± 5
78	13298	53	46.3	35 ± 6
78	15385	53	51.6	34 ± 5
*78	28683	106	101.8	36 ± 4
88	15519	48	45.1	29 ± 5
98	12480	24	22.6	18 ± 4
108	12926	15	14.0	11 ± 3
118	20300	15	11.8	5.8 ± 1.9
128	12129	2	2	1.6 ± 1.6

@ Corrected Neutron-Proton Coincidences = $(N+P) - (N_{II}+P)\dfrac{N_I}{N_{II}}$

#Normalized corrected neutron-proton coincidences = $\dfrac{1}{P_I}$ X Corrected Coincidences

*Combination of runs above at same angle

Taken with proton counter at 76 ± 5 degrees and with proton energy of 130 ± 12 Mev.

See Table II for data on Target

TABLE IVa

Summary of Carbon Data

Neutron Counter Angle (θ_N)	Proton Counts (P_1)	Neutron – Proton Coincidences		
		Total (N+P)	Corrected@	Normalized Corrected#
38	13248	11	3.4	6.3 ± 2.9
48	8020	9	8.0	10 ± 4
58	13785	30	25.3	19 ± 4
68	13684	43	38.9	29 ± 5
78	13298	53	46.[illegible]	35 ± 6
78	15385	53	51.6	34 ± 5
*78	28683	105	101.8	36 ± 4
88	15519	48	45.1	29 ± 5
98	12480	24	22.6	18 ± 4
108	12926	15	14.0	11 ± 3
118	20900	15	11.8	5.8 ± 1.9
128	12129	2	2	1.6 ± 1.6

@ Corrected Neutron-Proton Coincidences = $(N+P) - (N_{II}+P)\frac{N_I}{N_{II}}$

#Normalized corrected neutron-proton coincidences = $\frac{1}{P_1}$ X Corrected Coincidences

*Combination of runs at same angle

Taken with proton counter at 76 ± 5 degrees and with proton energy of 130 ± 12 Mev.

See Table II for data on Target.

TABLE IVd

Summary of Light Water (Oxygen) Data

Neutron Counter Angle (Θ_N)	Proton Counts (P_I)	Neutron - Proton Coincidences		
		Total (N+P)	Corrected@	Normalized# Corrected
68	10694	32	26.2	25 ± 5
78	10527	46	38.1	36 ± 7
88	10646	25	22.4	21 ± 5
ave	10622			

@ Corrected Neutron-Proton Coincidences = $(N + P) - (N_{II} + P)\frac{N_I}{N_{II}}$

Normalized corrected neutron-proton coincidences = $\frac{1}{P_I}$ X Corrected Coincidences

Taken with proton counter at 76 ± 5 degrees and with proton energy of 130 ± 12 Mev.

See Table II for data on Target

TABLE IVd

Summary of Light Water (Oxygen) Data

Neutron Counter Angle (Θ_N)	Proton Counts (P_T)	Neutron - Proton Coincidences		
		Total (NTP)	Corrected@	Normalized Corrected#
68	10694	39	26.2	25 ± 6
78	10527	46	38.1	36 ± 7
88	10645	25	22.4	21 ± 5
ave	10622			

@ Corrected Neutron-Proton Coincidences = $(N\,P) - (N_{II}\,P)\frac{N_I}{N_{II}}$

Normalized corrected neutron-proton coincidences = $\frac{1}{P_T}$ X Corrected Coincidences

Taken with proton counter at 76 ± 5 degrees and with proton energy of 130 ± 12 Mev.

See Table II for data on Target

TABLE IVe

Summary of Aluminum Data

Neutron Counter Angle (Θ_N)	Proton Counts (P_I)	Neutron - Proton Coincidences		
		Total (N^+P)	Corrected@	Normalized Corrected#
38	14663	25	15.1	10 ± 4
58	15104	19	13.6	9 ± 3
68	14577	35	30.4	21 ± 4
78	14464	37	32.9	23 ± 4
78	14205	40	35.9	25 ± 5
*78	28669	77	68.8	24 ± 3
88	13963	27	23.4	17 ± 4
88	14135	36	32.4	23 ± 5
*88	28098	63	55.8	20 ± 3
98	12620	28	25.1	20 ± 4
98	12646	18	15.1	12 ± 4
*98	25266	46	40.2	15.9 ± 2.8
108	12717	14	11.3	9 ± 3
118	12975	12	9.5	7.3 ± 2.9
128	12556	9	6.7	5.3 ± 2.7

@ Corrected Neutron-Proton Coincidences = $(N^+P) - 0.005\, N_I$

Normalized corrected neutron-proton coincidences = $\frac{1}{P_I}$ X Corrected Coincidences

*Combination of runs above at same angle

Taken with proton counter at 76 ± 5 degrees and with proton energy of 130 ± 12 Mev.

See Table II for data on Target

TABLE IVa

Summary of Aluminum Data

Neutron Counter Angle (θ_N)	Proton Count (P_1)	Neutron - Proton Coincidences: Total (NP_1)	Corrected@	Normalized# Corrected
38	11653	25	15.1	10 ± 4
58	15104	19	13.6	9 ± 3
68	14577	35	30.4	21 ± 4
78	14464	37	32.9	23 ± 4
78	14205	40	35.9	25 ± 5
*78	28669	77	68.8	24 ± 3
88	13963	27	25.4	17 ± 4
88	14135	36	32.4	23 ± 5
*88	28098	63	55.8	20 ± 3
98	13620	28	25.1	20 ± 4
98	12646	18	15.1	12 ± 4
*98	25265	45	40.2	15.9 ± 2.8
108	12717	14	11.3	9 ± 3
118	12975	12	9.5	7.3 ± 2.9
128	12556	9	6.7	5.3 ± 2.7

@ Corrected Neutron-Proton Coincidences = $(NP_1) - 0.005\ N_1$

\# Normalized corrected neutron-proton coincidences = $\frac{1}{P_1}$ x Corrected Coincidences

*Combination of runs above at same angle

Taken with proton counter at 75 ± 5 degrees and with proton energy of 130 ± 12 Mev.

See Table II for data on Target

TABLE IVf

Summary of Copper Data

Neutron Counter Angle (Θ_N)	Proton Counts (P_I)	Neutron - Proton Coincidences		
		Total (N+P)	Corrected@	Normalized# Corrected
38	10556	15	(-) 9.7	(-) 9 ± 5
48	13929	16	10.4	7.5 ± 2.9
58	17493	29	22.9	13 ± 3
68	16197	35	32.3	20 ± 4
73	16451	27	23.5	14 ± 3
78	10800	16	14.9	14 ± 4
78	17166	38	34.0	20 ± 4
*78	27966	54	50.1	17.9 ± 2.7
88	16714	34	30.3	18 ± 3
98	16159	20	17.0	10.5 ± 2.9
108	16273	8	6.3	3.9 ± 1.8
118	16064	2	1.1	0.7 ± 0.9
128	15543	8	4.8	3.1 ± 1.9

@ Corrected Neutron-Proton Coincidences = $(N\,P) - (N_{II}\,P)\dfrac{N_I}{N_{II}}$

Normalized corrected neutron-proton coincidences = $\dfrac{1}{P_I}$ x Corrected Coincidences

* Combination of runs above at same angle

Taken with proton counter at 76 ± 5 degrees and with proton energy of 130 ± 12 Mev.

See Table II for data on Target

TABLE IV

Summary of Copper Data

Neutron Counter Angle (θ_N)	Proton Counts (P_I)	Neutron - Proton Coincidences Total (NP)	Corrected@	Normalized# Corrected
38	10596	15	(-) 9.[illegible]	(-) 9 ± 5
48	13929	16	10.4	7.5 ± 2.9
58	17493	29	22.9	13 ± 3
68	16197	35	32.3	20 ± 4
73	16451	27	23.5	14 ± 3
78	10800	16	14.9	14 ± 4
78	17166	38	34.0	20 ± 4
*78	27966	54	50.1	17.9 ± 2.7
88	16714	34	30.3	18 ± 3
98	16159	20	17.0	10.5 ± 2.9
108	16273	8	6.3	3.9 ± 1.8
118	16064	2	1.1	0.7 ± 0.9
128	15563	8	4.8	3.1 ± 1.9

@ Corrected Neutron-Proton Coincidences = $(N\,P) - (N_{II}\,P)\frac{N_I}{N_{II}}$

Normalized corrected neutron-proton coincidences = $\frac{1}{P_I}$ x Corrected Coincidences

* Combination of runs above at same angle

Taken with proton counter at 76 ± 5 degrees and with proton energy of 130 ± 12 Mev.

See Table II for data on Target

The factor 0.98 compensated for the different target thicknesses explained in Section II D. The reduction of data according to the above formula is illustrated in Table V. The denominator is an approximately 20 percent difference between the two proton rates. The denominator was obtained by averaging the proton rates at all angles. Despite this the error in the denominator for deuterium still was commensurate with the errors in the numerator at the various angles.

As the H_2O curve was fairly flat in the region of interest for deuterium previous experience had shown it was not necessary to run H_2O at every angle for the information desired in this experiment. Consequently, as all that was desired of the deuterium curve was to check the resolution of the geometry employed in these measurements the H_2O target was run only at 68, 78 and 88 degrees. The remaining data was filled in from two previously determined oxygen curves with almost identical geometries.

C. Resolution of Equipment

If the target had been infinitesimal in size the finite size of the proton counter and the neutron counter would have given a triangular resolution curve of about 10 degrees width at half height. The peak height from deuterium obtained in this case would have been the efficiency of the neutron counter $\left(\frac{\Delta N+P}{\Delta P}\right)$. Christie[31] has shown that the finite size of the target spreads out the resolution of the detecting system to about 14 degrees. The peak height is also decreased by the target size.

The factor 0.98 compensates for the different target thicknesses explained in Section II D. The reduction of data according to the above formula is illustrated in Table V. The denominator is an approximately 20 percent difference between the two proton rates. The denominator was obtained by averaging the proton rates at all angles. Despite this the error in the denominator for deuterium still was commensurate with the errors in the numerator at the various angles.

As the H_2O curve was fairly flat in the region of interest for deuterium previous experience had shown it was not necessary to run H_2O at every angle for the information desired in this experiment. Consequently, as all that was desired of the deuterium curve was to check the resolution of the geometry employed in these measurements the H_2O target was run only at 65, 75 and 85 degrees. The remaining data was filled in from two previously determined oxygen curves with almost identical geometries.

C. Resolution of Equipment

If the target had been infinitesimal in size the finite size of the proton counter and the neutron counter would have given a triangular resolution curve of about 10 degrees width at half height. The peak height from deuterium obtained in this case would have been the efficiency of the neutron counter $\left(\frac{\Delta\Omega\epsilon}{4\pi}\right)$. Christie[11] has shown that the finite size of the target spreads out the resolution of the detecting system to about 11 degrees. The peak height is also decreased by the target size.

TABLE V

Reduction of Data for Deuterium From D_2O and H_2O

Neutron Counter Angle θ_N	Neutron-Proton Coincidences				Average Proton Counts				Virtual Deuterium Coincidences X 103
	D_2O@	H_2O	$0.98xH_2O$	Difference $D_2O-0.98\ H_2O$	D_2O¢	H_2O&	$0.98\ H_2O$	Differences $D_2O-0.98H_2O$	
63	29.6		25.1#	8.1	12570	10622	10410	2160	3.8 ± 4.0
68	62.5	26.2	25.7*	36.8	"	"	"	"	17.0 ± 4.7
73	121.2		35.8#	85.4	"	"	"	"	40 ± 6
78	133.4	38.1	37.3*	96.1	"	"	"	"	45 ± 5
83	81.9		35.8#	46.1	"	"	"	"	21.4 ± 4.1
88	40.6	22.4	22.0*	18.6	"	"	"	"	8.6 ± 3.2

@ From Column 4 Table IVa

From previous oxygen data

* From Column 4 Table IVd

¢ See Table IVa

& See Table IVc

All data normalized to 3000 Mice

$$\text{Column 10} = \frac{(N_+P)_{D_2O} - 0.98\,(N_+P)_{H_2O}}{\text{Pave}_{D_2O} - 0.98\ \text{Pave}_{H_2O}} \times 10^3$$

The angular resolution of the detecting system introduced errors in the counting rates at Θ_N that are estimated to be less than three percent for all elements except lithium. In the case of lithium the error is estimated to be less than six percent. In calculating the results the finite resolution of the detecting system has been neglected. A more exact analysis should be made if a better theory is developed for the curve shapes. (See appendix I)

D. Reliability of the Data

The statistical spread in the data is large and is indicated on figures 6 through 11. As the process occurs more frequently in light nuclei (per gram of target) the counting rates were higher in the light nuclei and better statistics could be obtained. The statistical spread includes that associated with the subtraction of the accidental count. The accidental counting rate is an appreciable correction for the heavier elements especially at smaller neutron angles. In all elements except aluminum it seemed to be predictable on the basis of the resolving time of the equipment. In the case of aluminum the observed accidental rates were higher than the calculated values. When the aluminum data was corrected for the observed rate it was obvious that some failure had occurred in the circuit. For aluminum the calculated accidental rate as corroborated by the measurements on other elements was used.

The question of whether the curves go to zero at large angles from the center of the distribution or whether there is a constant

The angular resolution of the detecting system introduced errors in the counting rates at θ_x that are estimated to be less than three percent for all elements except lithium. In the case of lithium the error is estimated to be less than six percent. In calculating the results the finite resolution of the detecting system has been neglected. A more exact analysis should be made if a better theory is developed for the curve shapes. (See Appendix I)

D. Reliability of the Data

The statistical spread in the data is large and is indicated on figures 6 through 11. As the process occurs more frequently in light nuclei (per gram of target) the counting rates were higher in the light nuclei and better statistics could be obtained. The statistical spread includes that associated with the subtraction of the accidental count. The accidental counting rate is an appreciable correction for the heavier elements especially at smaller neutron angles. In all elements except aluminum it seemed to be predictable on the basis of the resolving time of the equipment. In the case of aluminum the observed accidental rates were higher than the calculated values. When the aluminum data was corrected for the observed rate it was obvious that some failure had occurred in the circuit. For aluminum the calculated accidental rate as corroborated by the measurements on other elements was used.

The question of whether the curves go to zero at large angles from the center of the distribution or whether there is a constant

(scattered) neutron background is very important in interpreting the results. For the light nuclei the curves were definitely observed to go to zero. However, in heavier nuclei (aluminum and copper) the accidental rate and poor statistics leave this question unresolved. Much longer runs and faster electronics circuitry than those employed would be needed to resolve this problem.

In that the ratios of $\frac{N+P}{P}$ were used in obtaining the widths of curves, the measurements were self monitoring. Very conveniently such a ratio removes errors that would arise from fluctuations or drifts in the proton detecting system, the machine's intensity, and the machine's energy. The only drift or fluctuation not taken care of by this ratio are those arising in the neutron detecting system. Studies of the neutron detector by Christie[31] indicated that it was not a rapidly varying function of the bias where it was run. The mixing of the order of running the different angles of the neutron counter should have removed any systematic errors in the shape of the curve that would have arisen from instrumental errors.

Electronic failures were not sources of errors due to the double scalers on the important counting rates and the frequent checking of standards.

In summary, the main sources of errors arising in the shapes of the curves are those associated with the accidental counting rates and counting statistics.

(scattered) neutron background is very important in interpreting the results. For the light nuclei the curves were definitely observed to go to zero. However, in heavier nuclei (aluminum and copper) the accidental rate and poor statistics leave this question unresolved. Much longer runs and faster electronics circuitry than those employed would be needed to resolve this problem.

In that the ratios of $\frac{N+P}{P}$ were used in obtaining the widths of curves, the measurements were self monitoring. Very conveniently such a ratio removes errors that would arise from fluctuations or drifts in the proton detecting system, the machine's intensity, and the machine's energy. The only drift or fluctuation not taken care of by this ratio are those arising in the neutron detecting system. Studies of the neutron detector by Christie[31] indicated that it was not a rapidly varying function of the bias where it was run. The mixing of the order of running the different angles of the neutron counter should have removed any systematic errors in the shape of the curve that would have arisen from instrumental errors.

Electronic failures were not sources of errors due to the double scalers on the important counting rates and the frequent checking of standards.

In summary, the main sources of errors arising in the shapes of the curves are those associated with the accidental counting rates and counting statistics.

V. Results

A. Deuterium

The angular distribution of neutrons in coincidence with protons from deuterium is shown in Figure 6 which plots the (subtracted) neutron-proton coincidences from deuterium normalized to the (subtracted) proton count of deuterium as the ordinate versus the angle of the neutron counter as the abscissa. These values are for a proton counter angle of 76 ± 5 degrees and a proton energy of 130 ± 12 Mev and are tabulated in the first and last columns of Table V. The deuterium curve is an experimental check on the angular and energy resolution of the telescopes as the deuteron in deuterium may be assumed at rest at the energies involved in this experiment. The full width at half height is 14 degrees which agrees with the value calculated from kinematics and the experimental arrangement[31]. This distribution went to zero on either side of its center.

B. Lithium

The angular distribution of neutrons in coincidence with protons from lithium is shown in Figure 7 which plots the neutron-proton coincidences from lithium normalized to the proton count from lithium as the ordinate versus the angle of the neutron counter as the abscissa. These values are tabulated in the first and last columns of Table IV b. A broadening of the width at half height to 30 degrees is noted. Here a true angular spread in the neutron distribution is seen which is

V. Results

A. Deuterium

The angular distribution of neutrons in coincidence with protons from deuterium is shown in Figure 6 which plots the (subtracted) neutron-proton coincidences from deuterium normalized to the (subtracted) proton count of deuterium as the ordinate versus the angle of the neutron counter as the abscissa. These values are for a proton counter angle of 76 $\pm$ 5 degrees and a proton energy of 130 $\pm$ 12 Mev and are tabulated in the first and last columns of Table V. The deuterium curve is an experimental check on the angular and energy resolution of the telescopes as the deuteron in deuterium may be assumed at rest at the energies involved in this experiment. The full width at half height is 14 degrees which agrees with the value calculated from kinematics and the experimental arrangement[21]. This distribution went to zero on either side of its center.

B. Lithium

The angular distribution of neutrons in coincidence with protons from lithium is shown in Figure 7 which plots the neutron-proton coincidences from lithium normalized to the proton count from lithium as the ordinate versus the angle of the neutron counter as the abscissa. These values are tabulated in the first and last columns of Table IV b. A broadening of the width at half height to 30 degrees is noted. Here a true angular spread in the neutron distribution is seen which is

Figure 6

Neutron-Proton Coincidences from Deuterium

This is a plot of (subtracted) neutron-proton coincidences from deuterium normalized to the (subtracted) proton count from deuterium times 10^3 versus the angle of the neutron counter.

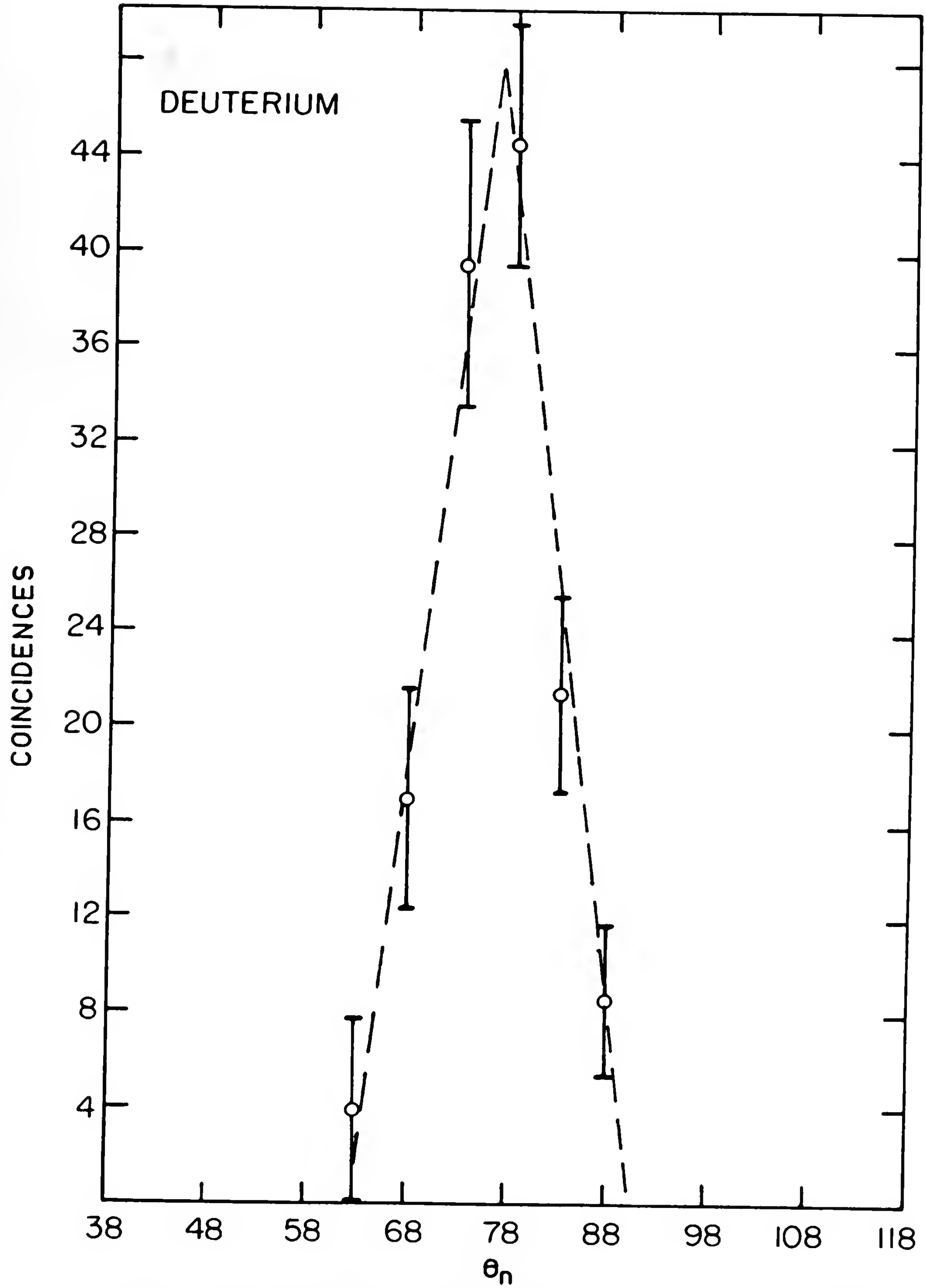

NEUTRON PROTON COINCIDENCES FROM DEUTERIUM

Figure 6

Figure 7

Neutron-Proton Coincidences from Lithium

This is a plot of neutron-proton coincidences from lithium normalized to the proton count from lithium times 10^4 versus the angle of the neutron counter.

Figure 7

Neutron-Proton Coincidences from Lithium

This is a plot of neutron-proton coinci-
dences from lithium normalized to the
proton count from lithium times 10^4 versus
the angle of the neutron counter.

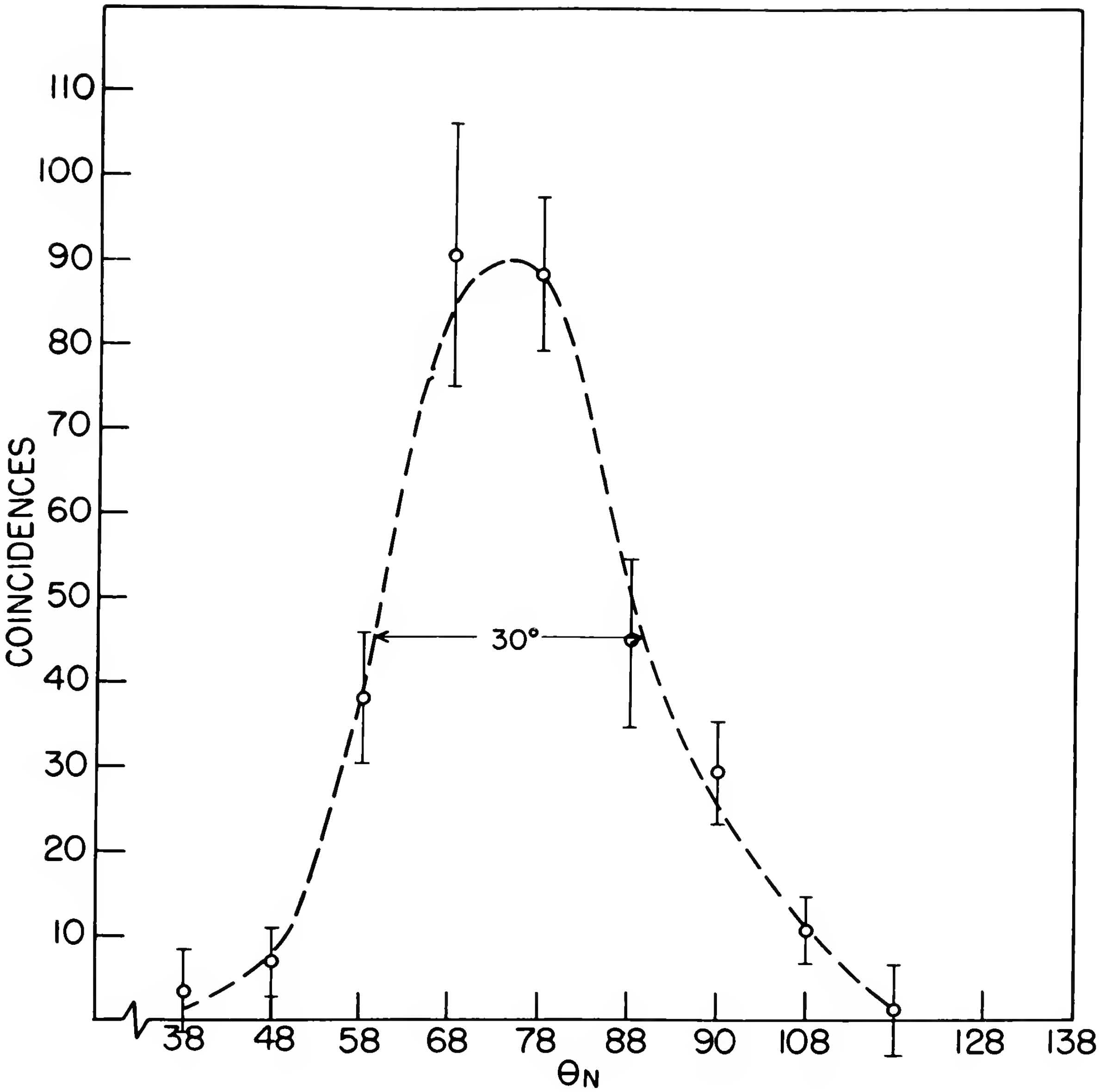

NEUTRON PROTON COINCIDENCES FROM LITHIUM

Figure 7

attributed to the presence of a finite momentum distribution within the nucleus for this type of experiment. This curve is in close agreement with that obtained by Barton and Smith[31]. The lithium curve went to zero on both sides of the distribution.

C. Carbon

The angular distribution of neutrons in coincidence with protons from carbon is shown in Figure 8 which is the same type of plot as Figure 7 with the values obtained from the first and last columns of Table IVc. A further broadening of the half width to 41 degrees is noted indicating a greater spread in the momentum distribution over that found in lithium. Sufficient data was not taken at large angles from the center of the distribution to ascertain if the curve went to zero.

D. Oxygen

Only the amount of light water data (hence oxygen data in neutron-proton scattering by gamma rays) required for the D_2O - H_2O subtraction for deuterium was taken during this work. However, the curve shown in Figure 9 which is a similar plot to Figure 7 was made up partly of data from previous work in this laboratory (published[34] and unpublished). The values plotted from this work are found in the first and last columns of Table IVd. Here the width at half height is 36 degrees which is not significantly different from that of carbon. The data has not been normalized in any way. This shows the reproducibility of such measurements over a period of six months. It should also

attributed to the presence of a finite momentum distribution within the nucleus for this type of experiment. This curve is in close agreement with that obtained by Barton and Smith[31]. The lithium curve went to zero on both sides of the distribution.

C. Carbon

The angular distribution of neutrons in coincidence with protons from carbon is shown in Figure 8 which is the same type of plot as Figure 7 with the values obtained from the first and last columns of Table IVc. A further broadening of the half width to 41 degrees is noted indicating a greater spread in the momentum distribution over that found in lithium. Sufficient data was not taken at large angles from the center of the distribution to ascertain if the curve went to zero.

D. Oxygen

Only the amount of light water data (hence oxygen data in neutron-proton scattering by gamma rays) required for the $D_2O - H_2O$ subtraction for deuterium was taken during this work. However, the curve shown in Figure 9 which is a similar plot to Figure 7 was made up partly of data from previous work in this laboratory (published[34] and unpublished). The values plotted from this work are found in the first and last columns of Table IVd. Here the width at half height is 36 degrees which is not significantly different from that of carbon. The data has not been normalized in any way. This shows the reproducibility of such measurements over a period of six months. It should also

Figure 8

Neutron-Proton Coincidences from Carbon

This is a plot of neutron-proton coincidences from carbon normalized to the proton count from carbon times 10^4 versus the angle of the neutron counter.

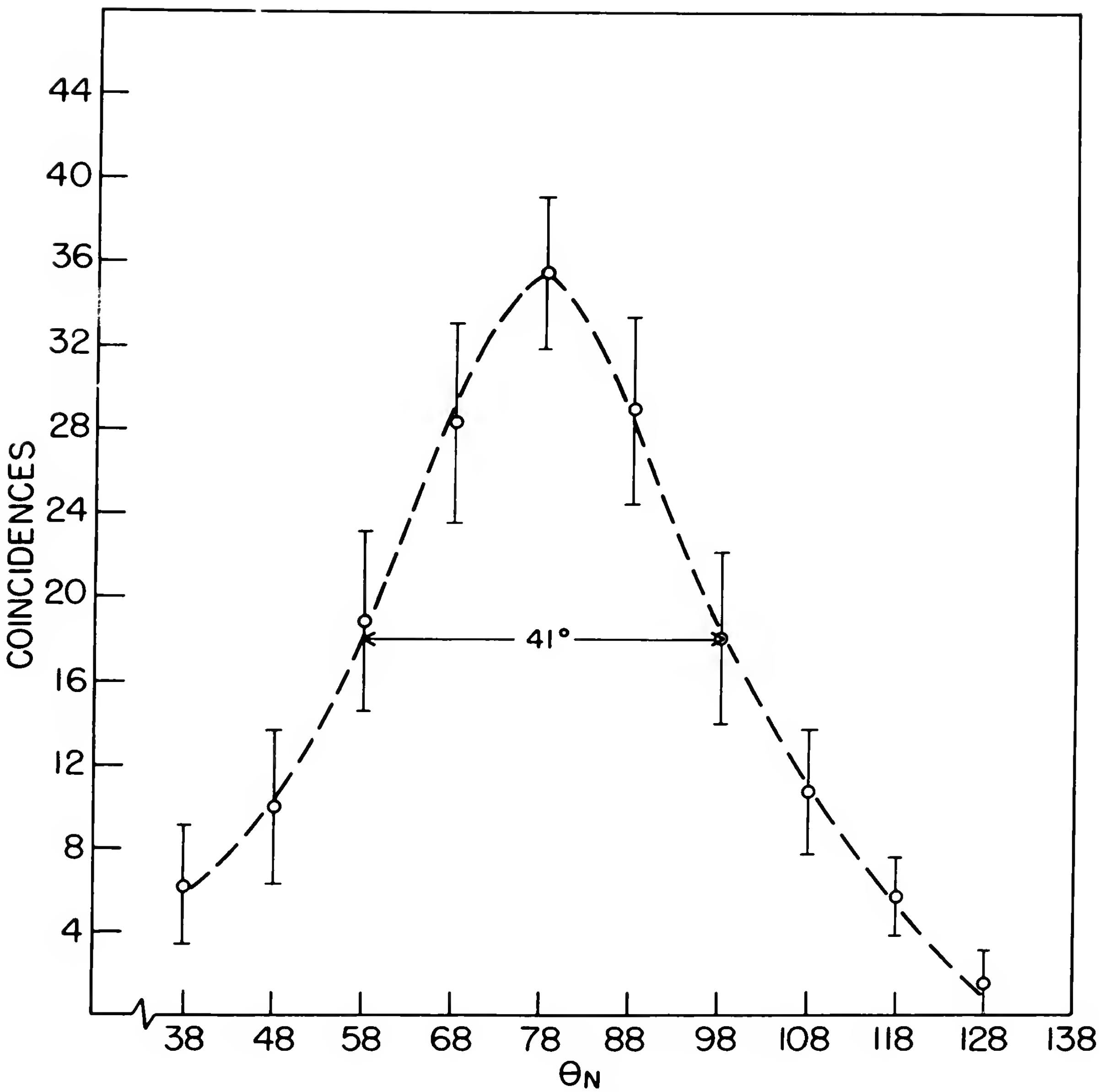

NEUTRON PROTON COINCIDENCES FROM CARBON

Figure 8

Figure 9

Neutron-Proton Coincidences from Oxygen

This is a plot of neutron-proton coincidences from oxygen normalized to the proton count from oxygen times 10^4 versus the angle of the neutron counter.

Figure 9

Neutron-Proton Coincidences from Oxygen

This is a plot of neutron-proton coinci-
dences from oxygen normalized to the
proton count from oxygen times 10^4 versus
the angle of the neutron counter.

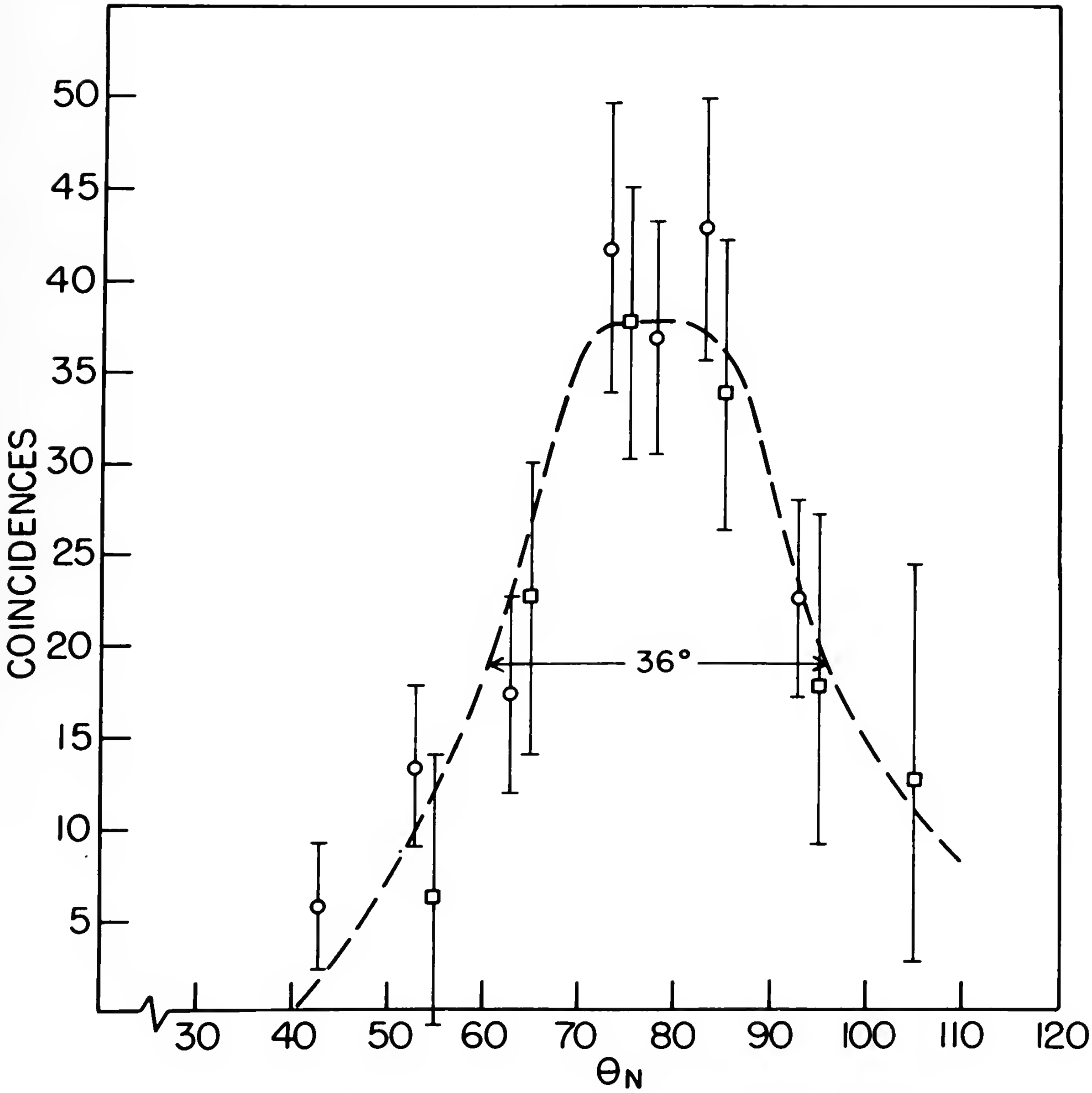

NEUTRON PROTON COINCIDENCES FROM OXYGEN

Figure 9

be noted that the statistical errors are larger than those in the other elements. The curve was carried to low enough angles to ascertain that it went to zero.

E. Aluminum

The angular distribution of neutrons in coincidence with protons from aluminum is shown in Figure 10 which is a similar plot to Figure 7 with the values obtained from the first and last columns of Table IVe. An apparent error* was introduced into the aluminum data due to lowering the bias on the delayed neutron channel too far resulting in an erroneous accidental counting rate. This was corrected by using an average accidental counting rate based on the normal neutron counting rate as shown in Table IVe. Insufficient data was obtained to determine whether this curve went to zero on either side of the distribution.

F. Copper

The angular distribution of neutrons in coincidence with protons from copper is shown in Figure 11 which is a similar plot to Figure 7 with the values obtained from the first and last columns of Table IVf. Here the width at half height is 49 degrees which is not significantly different from that of aluminum. The statistical error in the data made it uncertain whether the curve goes to zero on either side of the distribution.

*See Section IVC

be noted that the statistical errors are larger than those in the other elements. The curve was carried to low enough angles to ascertain that it went to zero.

E. Aluminum

The angular distribution of neutrons in coincidence with protons from aluminum is shown in Figure 10 which is a similar plot to Figure 7 with the values obtained from the first and last columns of Table IVe. An apparent error* was introduced into the aluminum data due to lowering the bias on the delayed neutron channel too far resulting in an erroneous accidental counting rate. This was corrected by using an average accidental counting rate based on the normal neutron counting rate as shown in Table IVe. Insufficient data was obtained to determine whether this curve went to zero on either side of the distribution.

F. Copper

The angular distribution of neutrons in coincidence with protons from copper is shown in Figure 11 which is a similar plot to Figure 7 with the values obtained from the first and last columns of Table IVf. Here the width at half height is 69 degrees which is not significantly different from that of aluminum. The statistical error in the data made it uncertain whether the curve goes to zero on either side of the distribution.

*See Section IVC

Figure 10

Neutron-Proton Coincidences from Aluminum

This is a plot of neutron-proton coincidences from aluminum normalized to the proton count from aluminum times 10^4 versus the angle of the neutron counter.

Figure 10

Neutron-Proton Coincidences from Aluminum

This is a plot of neutron-proton coincidences from aluminum normalized to the proton count from aluminum times 10^4 versus the angle of the neutron counter.

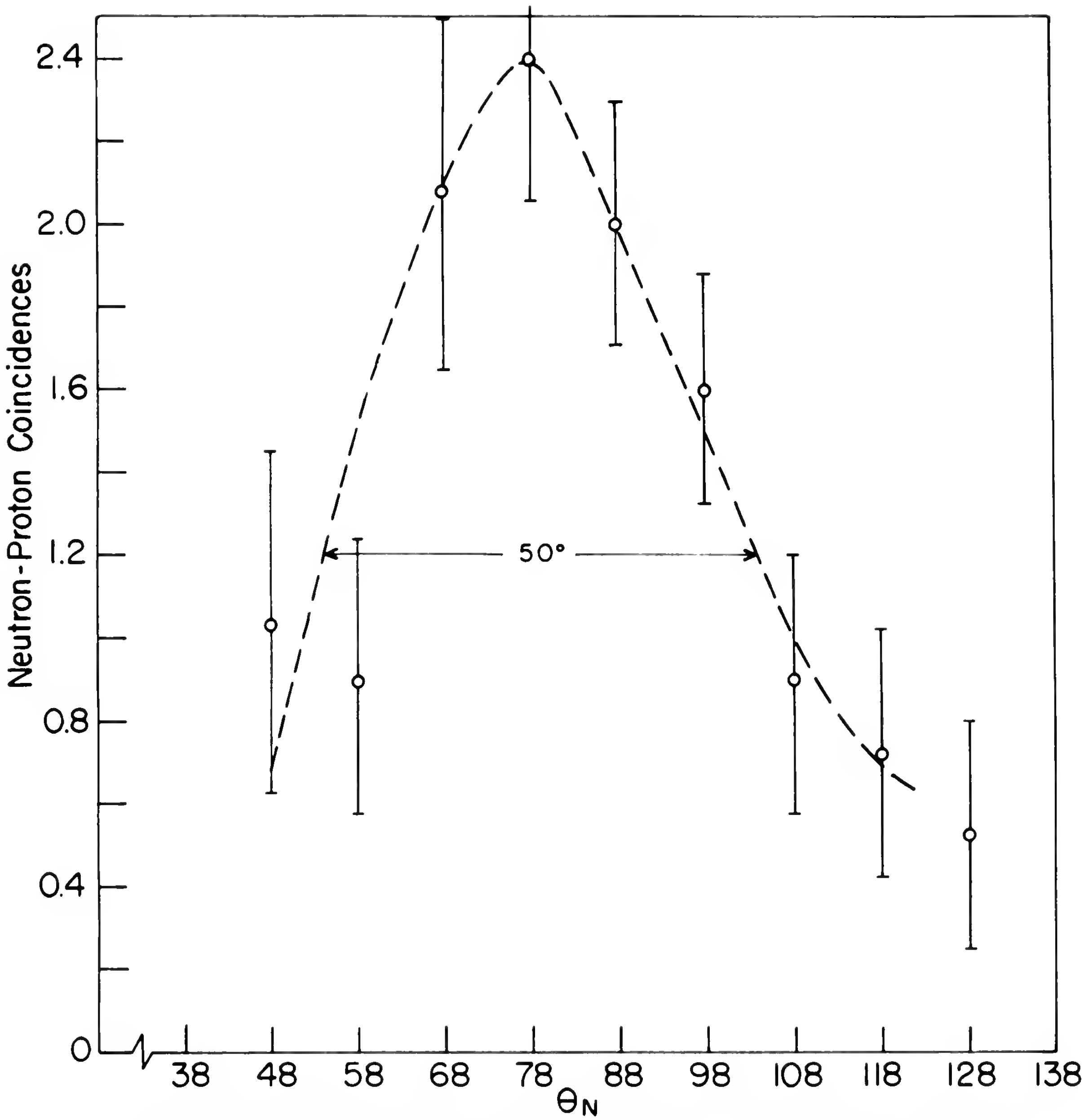

NEUTRON PROTON COINCIDENCES FROM ALUMINUM

Figure 10

Figure 11

Neutron-Proton Coincidences from Copper

This is a plot of neutron-proton coincidences from copper normalized to the proton count from copper times 10^4 versus the angle of the neutron counter.

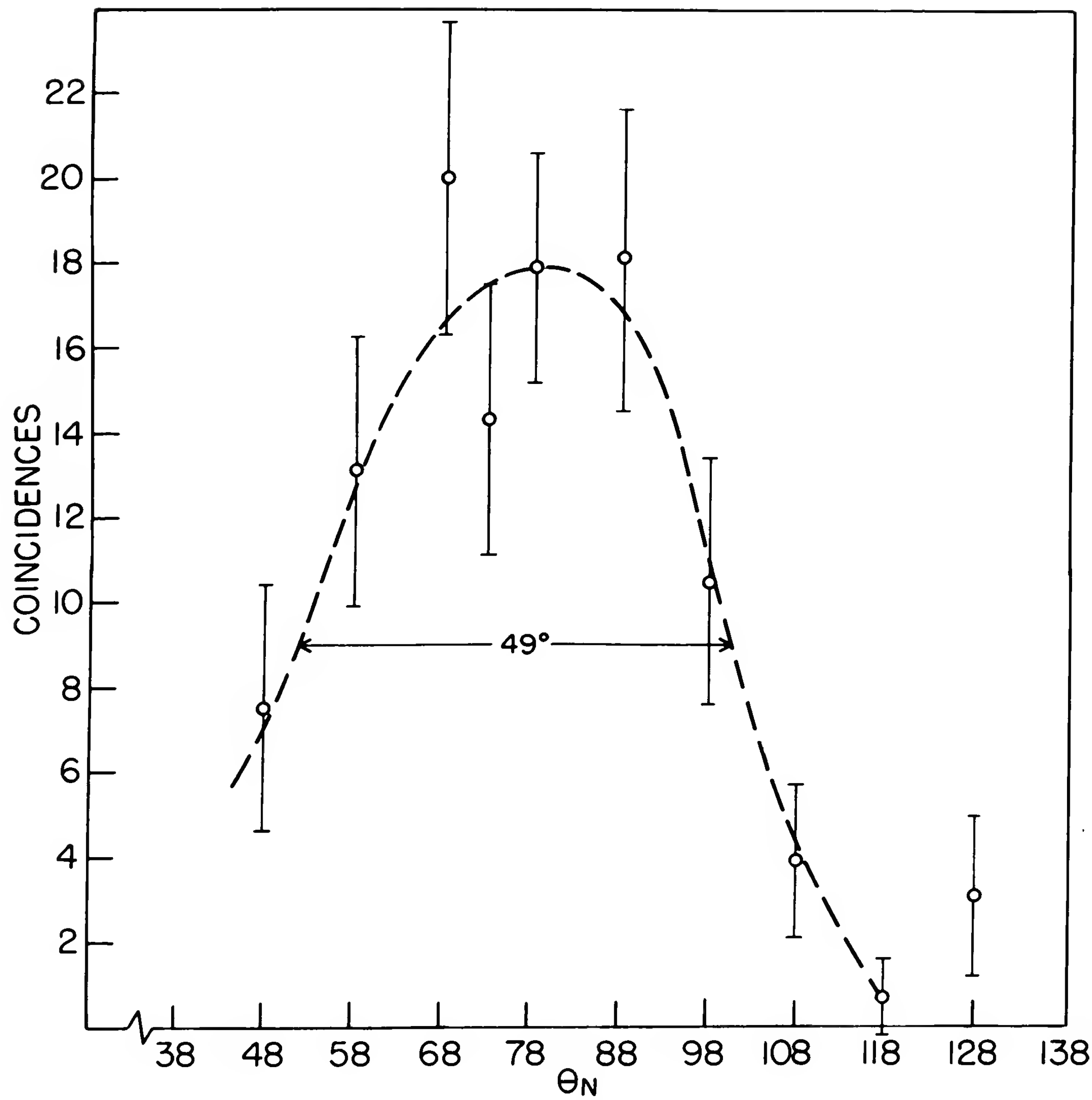

NEUTRON PROTON COINCIDENCES FROM COPPER

Figure 11

VI. Conclusions

The purpose of this work was to employ the quasi-deuteron model of Levinger[6] as a mode of studying nuclear internal momenta. As an incidental result the quasi-deuteron model was substantially established with better data on more elements.

The detection of an angular spread in lithium beyond that due to the resolution of the detectors indicated the presence of a finite momentum distribution. A marked increase in the spread of the distribution occurred between lithium and carbon indicating an increase in the average momentum of the nucleons. However, the increase in the spread from carbon to aluminum and copper was slight. This does not necessarily indicate an increase in the average momentum since this slight increase could well be attributed to scattering of the neutrons within the nucleus.

A first approximation to a quantative explanation of the shape of the angular distributions obtained has been derived by Wattenberg (see Appendix I). It is based on the assumptions that the nucleons in the nucleus have a three-dimensional gaussian momentum distribution, that neutrons and protons have the same momentum distributions, that it is possible to combine momenta and neglect the conservation of energy, and that the scattering of nucleons inside the nucleus can be neglected. The last assumption causes the calculated distribution to become less reliable with increasing atomic number as the effect of scattering becomes more pronounced with increasing nuclear dimensions.

VI. Conclusions

The purpose of this work was to employ the quasi-deuteron model of Levinger[6] as a mode of studying nuclear internal momenta. As an incidental result the quasi-deuteron model was substantially established with better data on more elements.

The detection of an angular spread in lithium beyond that due to the resolution of the detectors indicates the presence of a finite momentum distribution. A marked increase in the spread of the distribution occurred between lithium and carbon indicating an increase in the average momentum of the nucleons. However, the increase in the spread from carbon to aluminum and copper was slight. This does not necessarily indicate an increase in the average momentum since this slight increase could well be attributed to scattering of the neutrons within the nucleus.

A first approximation to a quantitative explanation of the shape of the angular distributions obtained has been derived by Wattenberg (see Appendix I). It is based on the assumptions that the nucleons in the nucleus have a three-dimensional gaussian momentum distribution, that neutrons and protons have the same momentum distributions, that it is possible to combine momenta and neglect the conservation of energy, and that the scattering of nucleons inside the nucleus can be neglected. The last assumption causes the calculated distribution to become less reliable with increasing atomic number as the effect of scattering becomes more pronounced with increasing nuclear dimensions.

With the above assumptions and neglecting the finite resolution of the detectors the curve would have a distribution about the midpoint given by

$$N(\psi)\sin\psi\, d\psi = N_0 e^{-\frac{\sin^2\psi}{\sin^2\psi_0}}\left(\frac{\sin^2\psi_0}{2}+\cos^2\psi\right)\sin\psi\, d\psi$$

where ψ is the angle from the midpoint of the distribution (78 degrees) and $\sin^2\psi_0 = \frac{2E_g}{E_p}$ where E_p is the energy of the proton in the laboratory and E_g is the 1/e value of the initial gaussian distribution of the momenta of the nucleons in the nucleus. The term $\frac{\sin^2\psi_0}{2}$ can generally be neglected as being of the order of 0.1

Figure 12 shows a semilogarithmic plot of $\frac{\text{coincidences}}{\cos^2\psi}$ vs $\sin^2\psi$ which should give a straight line on semilogarithmic paper within the accuracy of the experiment and the theory. Only lithium, carbon and oxygen are shown as the heavier elements possessed a rise in $\frac{\text{coincidences}}{\cos^2\psi}$ at larger ψ. The rise at large ψ in the heavier elements can be attributed to the incidence of scattering in the heavier nuclei. The values of E_g as obtained from the plot are 9 ± 1.5 Mev for lithium, 19 ± 1.5 Mev for carbon and approximately 19 Mev for oxygen. The oxygen plot suffers from being the result of two different collimations of the proton counter and in not being normalized. The uncertainty of ± 1.5 Mev on the lithium and carbon results were obtained from the extreme slopes which could be fitted to the data. It should be noted that the 1/e values obtained for these two elements are much more definitely fixed by this experiment than in previous works. However, the values obtained are in the neighborhood of those previously obtained for other

With the above assumptions and neglecting the finite resolution of the detectors the curve would have a distribution about the midpoint given by

$$N(\psi)\sin\psi\,d\psi = N_0 e^{-\frac{\sin^2\psi}{\sin^2\psi_0}}\left(\sin^2\frac{\psi_0}{2}+\cos^2\psi\right)\sin\psi\,d\psi$$

where ψ is the angle from the midpoint of the distribution (78 degrees) and $\sin^2\psi_0 = \frac{2E_g}{E_p}$ where E_p is the energy of the proton in the laboratory and E_g is the 1/e value of the initial gaussian distribution of the momenta of the nucleons in the nucleus. The term $\sin^2\frac{\psi_0}{2}$ can generally be neglected as being of the order of 0.1.

Figure 12 shows a semilogarithmic plot of $\frac{\text{coincidences}}{\cos^2\psi}$ vs $\sin^2\psi$ which should give a straight line on semilogarithmic paper within the accuracy of the experiment and the theory. Only lithium, carbon and oxygen are shown as the heavier elements possessed a rise in $\frac{\text{coincidences}}{\cos^2\psi}$ at larger ψ. The rise at large ψ in the heavier elements can be attributed to the incidence of scattering in the heavier nuclei. The values of E_g as obtained from the plot are 9 ± 1.5 Mev for lithium, 19 ± 1.5 Mev for carbon and approximately 19 Mev for oxygen. The oxygen plot suffers from being the result of two different collimations of the proton counter and in not being normalized. The uncertainty of $\pm$ 1.5 Mev on the lithium and carbon results were obtained from the extreme slopes which could be fitted to the data. It should be noted that the 1/e values obtained for these two elements are much more definitely fixed by this experiment than in previous works. However, the values obtained are in the neighborhood of those previously obtained for other

Figure 12

Fit of Experimental Data for Lithium, Carbon and Oxygen to Theoretical Curve Shape

This is a plot of $\frac{\text{coincidences}}{\cos^2 \psi}$ versus $\sin^2 \psi$ which should be a straight line within the errors of the experiment if the experimental results fit the theory.

Figure 12

Fit of Experimental Data for Lithium, Carbon and Oxygen to Theoretical Curve Shape

This is a plot of $\frac{\text{coincidences}}{\cos^2\psi}$ versus $\cos^2\psi$ which should be a straight line within the errors of the carbon if the experimental results fit the theory.

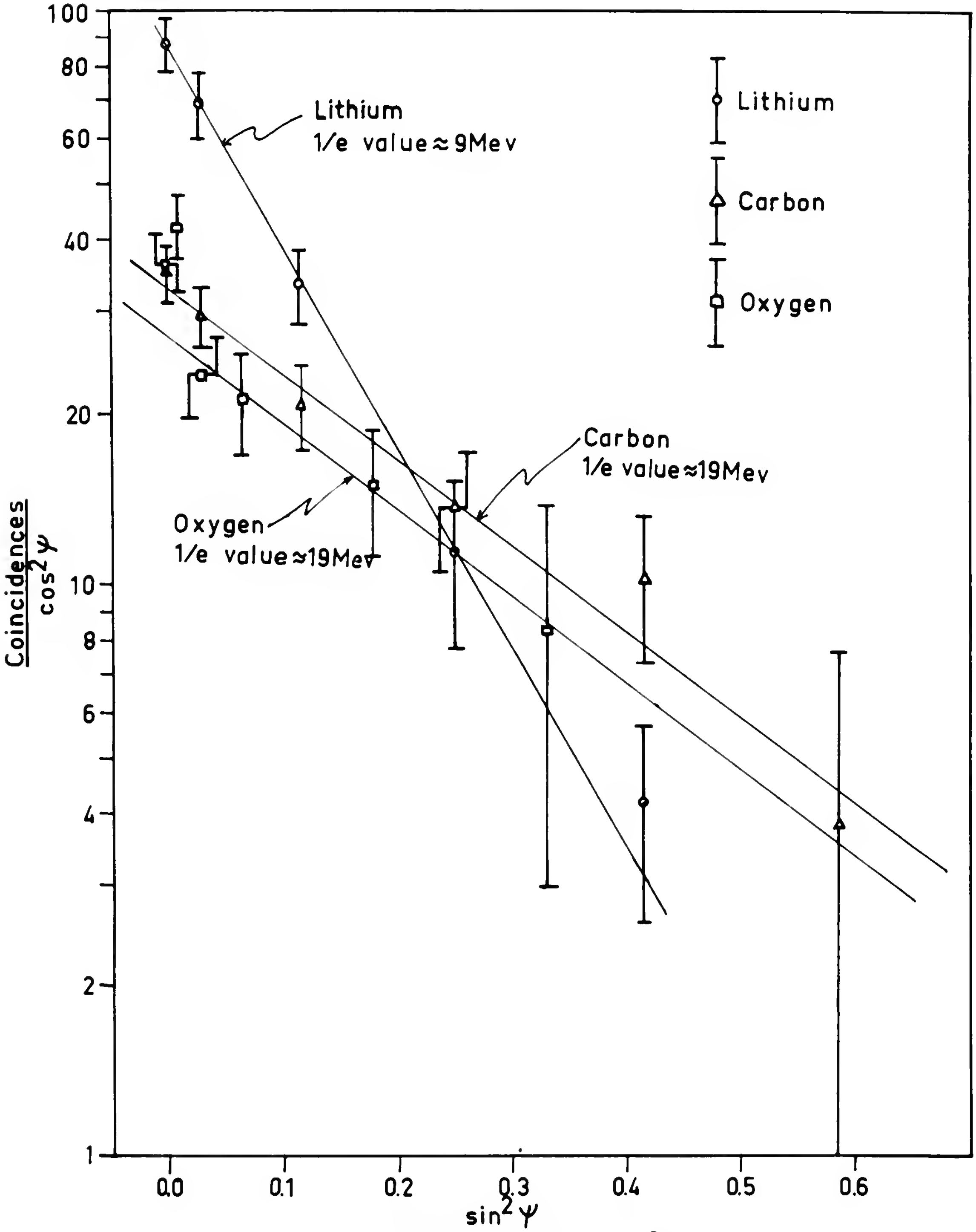

$\frac{\text{Coincidences}}{\cos^2\psi}$ vs. $\sin^2\psi$

Figure 12

light elements[22].

The reason for the apparent rise in the carbon and oxygen curves for small ψ is not clear. If it is not due to experimental causes, and if a more exact theory of the curve shapes should leave it unexplained, then the possibility exists that it is caused by nuclear shell effects.

Future work should undertake the examination of more nuclei (especially the heavier ones) and the extension of the observations over wider angles from the center of the distributions. With data from observations at larger angles from the midpoint of the distribution it may be possible to subtract off the scattered neutron background and hence obtain curves which may better fit the theory of Appendix I. Modification and improvement of the theory to include such effects as the scattered neutron background should be attempted.

BIBLIOGRAPHY

1. For a summary of work up to 1952 see K. Strauch, Ann. Rev. Nuclear Sci. 2, 105 (1953)

2. B. T. Feld, R. D. Godbole, A. Odian, F. Scherb, P. C. Stein and A. Wattenberg, Phys. Rev. 94, 1000 (1954). See this paper for references to other work.

3. C. Levinthal and A. Silverman, Phys. Rev. 82, 822 (1951)

4. D. Walker, Phys. Rev. 81, 634 (1951); 84, 149 (1951)

5. J. C. Keck, Phys. Rev. 85, 410 (1952)

6. J. S. Levinger, Phys. Rev. 84, 43 (1951)

7. J. W. Rosengren and J. M. Dudley, Phys. Rev. 89, 603 (1953)

8. A. M. Perry and J. C. Keck, Phys. Rev. 86, 629 (1952)

9. J. W. Weil and B. D. McDaniel, Phys. Rev. 92, 391 (1953)

10. T. S. Benedict and W. M. Woodward, Phys. Rev. 85, 924 (1952)

11. W. S. Gilbert and J. W. Rosengren, Phys. Rev. 88, 901 (1952)

12. H. Myers, A. Odian, P. C. Stein and A. Wattenberg, Phys. Rev. 95, 576 (1954)

13. M. Q. Barton and J. H. Smith, Phys. Rev. 95, 573 (1954)

14. M. Wiener, Energy and Angle Distribution of the Photoprotons from Deuterium, National Bureau of Standards Circular 515, U. S. Government Printing Office (1951)

15. E. Fermi, Jay Orear, A. H. Rosenfeld and R. A. Schluter, Nuclear Physics, University of Chicago Press, 1950, p. 159

16. G. F. Chew and M. L. Goldberger, Phys. Rev. 77, 470 (1950)

17. For a discussion of nuclear radii see R. D. Evans, The Atomic Nucleus, McGraw-Hill Book Co. Inc. (1955) Chapter II

18. J. Hadley and H. F. York, Phys. Rev. 80, 345 (1950)

19. J. Heidman, Phys. Rev. 80, 171 (1950)

20. O. Chamberlain and E. Segrè, Phys. Rev. 87, 81 (1952)

BIBLIOGRAPHY

1. For a summary of work up to 1952 see E. Strauch, Ann. Rev. Nuclear Sci. 2, 105 (1953)
2. B. T. Feld, R. D. Godbole, A. Odian, F. Scherb, P. C. Stein and A. Wattenberg, Phys. Rev. 94, 1000 (1954). See this paper for references to other work.
3. C. Levinthal and A. Silverman, Phys. Rev. 82, 822 (1951)
4. D. Walker, Phys. Rev. 81, 634 (1951); 84, 149 (1951)
5. J. C. Keck, Phys. Rev. 85, 410 (1952)
6. J. S. Levinger, Phys. Rev. 84, 43 (1951)
7. J. W. Rosengren and J. M. Dudley, Phys. Rev. 89, 603 (1953)
8. A. M. Perry and J. C. Keck, Phys. Rev. 86, 629 (1952)
9. J. W. Weil and B. D. McDaniel, Phys. Rev. 92, 391 (1953)
10. T. S. Benedict and W. M. Woodward, Phys. Rev. 85, 924 (1952)
11. W. S. Gilbert and J. W. Rosengren, Phys. Rev. 88, 901 (1952)
12. H. Myers, A. Odian, P. C. Stein and A. Wattenberg, Phys. Rev. 95, 576 (1954)
13. M. Q. Barton and J. H. Smith, Phys. Rev. 95, 573 (1954)
14. M. Wiener, Energy and Angle Distribution of the Photoprotons from Deuterium, National Bureau of Standards Circular 515, U. S. Government Printing Office (1951)
15. E. Fermi, Jay Orear, A. H. Rosenfeld and R. A. Schluter, Nuclear Physics, University of Chicago Press, 1950, p. 159
16. G. F. Chew and M. L. Goldberger, Phys. Rev. 77, 470 (1950)
17. For a discussion of nuclear radii see R. D. Evans, The Atomic Nucleus, McGraw-Hill Book Co. Inc. (1955) Chapter II
18. J. Hadley and H. F. York, Phys. Rev. 80, 345 (1950)
19. J. Heidmann, Phys. Rev. 80, 171 (1950)
20. O. Chamberlain and E. Segrè, Phys. Rev. 87, 81 (1952)

21. J. B. Cladis (Thesis), University of California Radiation Laboratory Report No. 1621 and J. B. Cladis, W. N. Hess and B. J. Moyer, Phys. Rev. 87, 425 (1952)

22. J. M. Wilcox (Thesis), University of California Radiation Laboratory Report No. 2540 (1954)

23. W. G. McMillan and E. Teller, Phys. Rev. 72, 1 (1947)

24. E. Henley and R. Huddlestone, Phys. Rev. 82, 754 (1951)

25. E. M. Henley, Phys. Rev. 85, 204 (1952)

26. M. M. Block, S. Passman and W. W. Havens, Phys. Rev. 83, 167 (1951)

27. M. M. Block, S. Passman and W. W. Havens, Phys. Rev. 88, 1239 (1952)

28. R. Bjorklund, W. E. Crandall, B. J. Moyer and H. F. York, Phys. Rev. 77, 213 (1950)

29. J. Steinberger and A. S. Bishop, Phys. Rev. 78, 494 (1950)

30. M. Lax and H. Feshback, Phys. Rev. 81, 189 (195

31. E. R. Christie (Thesis) M.I.T., Unpublished (1955)

32. A. C. Odian (Thesis) M.I.T., Unpublished (1955)

33. H. C. Ratz (Thesis) M.I.T., Unpublished (1952)

34. A. C. Odian, W. A. Rankin, P. C. Stein and A. Wattenberg, M.I.T. Laboratory for Nuclear Science Progress Report November 30, 1954, Page 30

21. J. B. Cladis (Thesis), University of California Radiation Laboratory Report No. 1621 and J. B. Cladis, W. N. Hess and B. J. Moyer, Phys. Rev. 87, 425 (1952)

22. J. M. Wilcox (Thesis), University of California Radiation Laboratory Report No. 2540 (1954)

23. W. G. McMillan and E. Teller, Phys. Rev. 72, 1 (1947)

24. E. Henley and R. Huddlestone, Phys. Rev. 82, 754 (1951)

25. E. M. Henley, Phys. Rev. 85, 204 (1952)

26. M. M. Block, S. Passman and W. W. Havens, Phys. Rev 83, 167 (1951)

27. M. M. Block, S. Passman and W. W. Havens, Phys. Rev. 88, 1239 (1952)

28. R. Bjorklund, W. E. Crandall, B. J. Moyer and H. F. York. Phys. Rev. 77, 213 (1950)

29. J. Steinberger and A. S. Bishop, Phys. Rev. 78, 494 (1950)

30. M. Lax and H. Feshbach, Phys. Rev. 81, 189 (195

31. E. R. Christie (Thesis) M.I.T., unpublished (1955)

32. A. C. Odian (Thesis) M.I.T., unpublished (1955)

33. H. G. Rate (Thesis) M.I.T., unpublished (1952)

34. A. C. Odian, W. A. Rankin, P. C. Stein and A. Wattenberg, M.I.T. Laboratory for Nuclear Science Progress Report November 30, 1954, page 30

Appendix I

A Crude Theory of the Neutron-Proton Coincidence Curve Shapes

(Developed by Dr. A. Wattenberg)

Assume momentum is that of a ground state of an harmonic oscillator potential; then, for the proton

$$\phi(p) = N e^{-\frac{p_x^2+p_y^2+p_z^2}{2p_0^2}}$$

where N is a normalizing constant

The density in momentum space is

$$\phi^*(p)\,\phi(p)\,dp_x dp_y dp_z = N^2 e^{-\frac{p_x^2+p_y^2+p_z^2}{p_0^2}}\,dp_x dp_y dp_z \quad (1)$$

Similarly for the neutron momentum density

$$\phi^*(q)\,\phi(q)\,dq_x dq_y dq_z = N^2 e^{-\frac{q_x^2+q_y^2+q_z^2}{q_0^2}}\,dq_x dq_y dq_z$$

The momentum density of the pair of particles is

$$N^4 e^{-\frac{p_x^2+q_x^2+p_y^2+q_y^2+p_z^2+q_z^2}{p_0^2}}\,dp_x dq_x dp_y dq_y dp_z dq_z \quad (2)$$

assuming $p_0 = q_0$

Let $\vec{P} = \vec{p} + \vec{q}$ $\qquad \vec{Q} = \vec{p} - \vec{q}$

$P_x = p_x + q_x \qquad Q_x = p_x - q_x$

$P_y = p_y + q_y \qquad Q_y = p_y - q_y$

$P_z = p_z + q_z \qquad Q_z = p_z - q_z$

$$p_x = \frac{P_x + Q_x}{2} \qquad q_x = \frac{P_x - Q_x}{2}$$

Then

$$P_x^2 + Q_x^2 = p_x^2 + 2p_xq_x + q_x^2 + p_x^2 - 2p_xq_x + q_x^2$$
$$= 2p_x^2 + 2q_x^2$$

Or

$$p_x^2 + q_x^2 = \frac{P_x^2 + Q_x^2}{2}$$

$$dp_x\, dq_x = J\left(\frac{p_x . q_x}{P_x , Q_x}\right) dP_x\, dQ_x$$

$$J_x = \left|\left(\frac{\partial p_x}{\partial P_x}\right)\left(\frac{\partial q_x}{\partial Q_x}\right) - \left(\frac{\partial p_x}{\partial Q_x}\right)\left(\frac{\partial q_x}{\partial P_x}\right)\right|$$

$$= \left|\left(\tfrac{1}{2}\right)\left(-\tfrac{1}{2}\right) - \left(\tfrac{1}{2}\right)\left(\tfrac{1}{2}\right)\right| = \frac{1}{2}$$

Thus (2) becomes

$$N^4 e^{-\frac{P_x^2+Q_x^2+P_y^2+Q_y^2+P_z^2+Q_z^2}{2p_0^2}}\; J_x\, J_y\, J_z\, dP_x\, dP_y\, dP_z\, dQ_x\, dQ_y\, dQ_z$$

or $$N^4 e^{-\frac{P_x^2+P_y^2+P_z^2}{P_0^2}}\, dP_x\, dP_y\, dP_z \times \frac{1}{8} \times \iiint_{-\infty}^{\infty} e^{-\left(Q_x^2+Q_y^2+Q_z^2\right)}\, dQ_x\, dQ_y\, dQ_z$$

$$P_0 = 1.4\, p_0$$

or $$\left[\frac{N^4 P_0^3\, \pi^{3/2}}{8}\right] e^{-\frac{P_x^2+P_y^2+P_z^2}{P_0^2}}\, dP_x\, dP_y\, dP_z \qquad (3)$$

APPROXIMATE THREE-DIMENSIONAL CASE

Use cylindrical coordinates

Let $R^2 = P_x^2 + P_y^2$

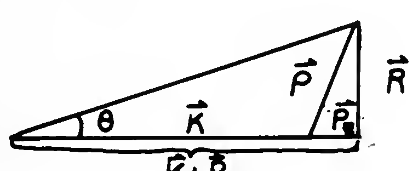

$$\iint dP_x\, dP_y = \int_0^\infty 2\pi R\, dR$$

$$P^2 = R^2 + P_z^2$$

$$\tan\theta = \frac{R}{K+P_z} \qquad 0 < \theta < \frac{\pi}{2}$$

Approximations $\quad \theta \ll 1 \quad K \gg P_z \quad$ then $R = K\theta$

(3) becomes

$$e^{-\frac{R^2}{P_o^2}} 2\pi R\, dR\, e^{-\frac{P_z^2}{P_o^2}} dP_z \quad (4)$$

$$R\,dR = K^2\theta\, d\theta$$

and (4) becomes

$$2\pi K^2 e^{-\frac{K^2\theta^2}{P_o^2}} \theta\, d\theta \int_{-\infty}^{\infty} e^{-\frac{P_z^2}{P_o^2}} dP_z$$

or $$2\pi K^2 P_o \sqrt{\pi}\, e^{-\frac{K_o^2}{P_o^2}\theta^2} \theta\, d\theta$$

Hence, the approximate three-dimensional curve shape is

$$e^{-\frac{K^2}{P_o^2}\theta^2} \theta\, d\theta \qquad 0<\theta<\frac{\pi}{2}$$

An exact three-dimensional curve shape has been derived in the following form:

$$2\pi^{3/2} P_o \left[\frac{P_o^2}{2} + K^2\cos^2\theta\right] \sin\theta\, e^{-\frac{K^2}{P_o^2}\sin^2\theta} d\theta \qquad 0<\theta<\frac{\pi}{2}$$

28993

Wilson

High energy photo-ejection of neutron-proton pairs from various nuclei.

Thesis
W636

28993

Wilson

High energy photo-ejection of neutron-proton pairs from various nuclei.